

T.C.
YEDİTEPE UNIVERSITY
INSTITUTE OF HEALTH SCIENCES
DEPARTMENT OF MEDICAL PHYSICS

**EFFECTS OF ITERATIVE RECONSTRUCTION ON
IMAGE QUALITY AND PATIENT DOSE IN
COMPUTED TOMOGRAPHY**

MASTER OF MEDICAL PHYSICS THESIS

ELİF ECEM ALCAN

SUPERVISOR

Prof. Dr. Ş. İpek KARAASLAN

CO-ADVISOR

Dr. Türkay TOKLU

İstanbul- 2019

THESIS APPROVAL FORM

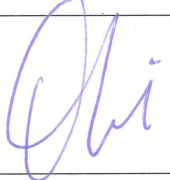
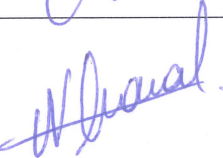
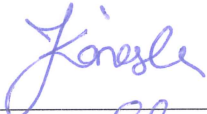


Institute : Yeditepe University Institute of Health Sciences
Programme : Health Physics
Title of the Thesis : Effects of Iterative Reconstruction on Image Quality and Patient

Dose in Computed Tomography

Owner of the Thesis : Elif Ecem ALCAN

Examination Date : 06.09.2019

This study have approved as a Master Thesisin regard to content and quality by the Jury.

	Title, Name-Surname (Institution)	(Signature)
Chair of the Jury:	Prof. Dr. Mustafa DEMİR (İSTANBUL ÜNİVERSİTESİ)	
Jury:	Prof. Dr. Nesrin ALTINSOY (İSTANBUL TEKNİK ÜNİVERSİTESİ)	
Supervisor:	Prof.Dr. Şerife İpek KARAASLAN (YEDİTEPE ÜNİVERSİTESİ)	
Co-advisor	Dr. Türkay TOKLU (YEDİTEPE ÜNİVERSİTESİ İHTİSAS HASTANESİ)	
Member/Examiner:	Doç. Dr. Nalan Alan Selçuk (YEDİTEPE ÜNİVERSİTESİ İHTİSAS HASTANESİ)	

APPROVAL

This thesis has been deemed by the jury in accordance with the relevant articles of Yeditepe University Graduate Education and Examinations Regulation and has been approved by Administrative Board of Institute with decision dated 18.12.2019.... and numbered ..2019/19-05

Director of Institute of Health Sciences


Prof. Dr. Bayram YILMAZ
Sağlık Bilimleri Enstitüsü Müdürü

DECLARATION

Bu tezin kendi çalışmam olduğunu, planlanmasından yazımına kadar hiçbir aşamasında etik dışı davranışımın olmadığını, tezdeki bütün bilgileri akademik ve etik kurallar içinde elde ettiğimi, tez çalışmasıyla elde edilmeyen bütün bilgi ve yorumlara kaynak gösterdiğimi ve bu kaynakları kaynaklar listesine aldığımı, tez çalışması ve yazımı sırasında patent ve telif haklarını ihlal edici bir davranışımın olmadığını beyan ederim.

Tarih

06.09.2019

ELİF ECEM ALCAN



ACKNOWLEDGMENTS

Tez çalışmamda ve eğitimim sırasında bilimsel katkı ve destek veren Yeditepe Üniversitesi Rektör Yardımcısı sayın Prof. Dr. Ş. İpek Karaaslan'a, Yeditepe Üniversitesi Öğretim Üyesi sayın Dr. Türkay Toklu'ya,

Sevgisi ve bilimsel bilgi desteği ile her zaman yanımda olan Yeditepe Üniversite Hastanesi Nükleer Tıp Ana Bilim Dalı Başkanı sayın Doç. Dr. Nalan Alan Selçuk'a,

Yüksek Lisans eğitimim süresince birlikte çalıştığım ve çalışma ortamımızda bana her zaman yardımcı olan tüm teknisyen arkadaşlarıma, hemşire, sekreter ve Yeditepe Üniversite Hastanesinde görevli tüm personele,

Bugüne kadar özveri ile maddi ve manevi desteğini hiçbir zaman benden esirgemeyen, eşim sevgili Mustafa Levent Alcan'a ve tüm aileme,

Her zaman varlığıyla beni güçlü kılan ve eğitim sürecimde destek veren oğlum Ömer Alcan'a

Sonsuz Teşekkürler...

TABLE OF CONTENTS

APPROVAL.....	ii
DECLARATION.....	iii
ACKNOWLEDGMENTS.....	iv
TABLE of CONTENT.....	v
LIST OF TABLES.....	vii
LIST OF FIGURES.....	viii
LIST OF SYMBOLS AND ABBREVIATIONS.....	xi
ABSTRACT.....	xii
ABSTRACT (Turkish).....	xiii
1. INTRODUCTION.....	1
2. GENERAL INFORMATION.....	3
2.1.History of Computed Tomography.....	3
2.2.General Principle of Computed Tomography.....	4
2.3.Image Reconstruction on Computed Tomography.....	15
2.3.1.Simple Back Projection (SBP).....	19
2.3.2.Filtered Back-Projection (FBP).....	20
2.3.3.Iterative Reconstruction (IR).....	22
2.3.3.1.ASIR (Adaptive Statistical Iterative Reconstruction).....	25
2.4.Haunsfield Unit Scale (windowing) on Computed Tomography.....	25
2.5. Dosimetric Parameters in Computed Tomography.....	26
2.5.1. Computed Tomography Dose Index (CTDI).....	27
2.5.1.1.Weighted Computerized Tomography Dose Index ($CTDI_w$).....	28
2.5.1.2.Volumetric Computed Tomography Dose Index ($CTDI_{vol}$).....	29
2.5.1.3.Dose Length Product (DLP).....	30
2.6. Image Quality Parameters in Computed Tomography.....	30
2.6.1. Noise on Computed Tomography.....	30
2.6.2. CT Number Accuracy.....	32
2.6.3. Low-Contrast Spatial Resolution.....	32
2.6.4. High-Contrast Spatial Resolution.....	33

3. MATERIALS AND METHODS.....	35
3.1.CTDI Measurements.....	35
3.2. Measurements for Image Quality Parameters.....	36
3.2.1.MTF Measurements.....	38
3.2.2.CNR Measurements.....	39
3.2.3.SNR Measurements.....	40
4.RESULTS and DISCUSSION.....	41
4.1. CTDI Measurements.....	41
4.2. MTF Measurements.....	43
4.3. CNR Measurements.....	49
4.4. SNR Measurements.....	55
5.CONCLUSIONS.....	59
6. REFERENCES.....	60
7. APPENDICES.....	62

LIST OF TABLES

Table 2.1. Summary of CT History.....	3
Table 2.2. Summary of CT Generations.....	14
Table 4.1. CTDI Result of 65 mA.....	42
Table 4.2. CTDI Result of 125 mA.....	42
Table 4.3. CTDI Result of 255 mA.....	43
Table 4.4. Summary of CTDI measurements.....	43



LIST OF FIGURES

Figure 2.1. Computed Tomography.....	4
Figure 2.2. Collimated Beam.....	4
Figure 2.3. Creation CT projected image.....	5
Figure 2.4. CT Projection Geometry.....	5
Figure 2.5. Attenuated Coefficient of CT.....	6
Figure 2.6. Mathematical process of Image Reconstruction.....	7
Figure 2.7. Pixels on CT images.....	7
Figure 2.8. Voxel on CT images.....	8
Figure 2.9. First (a) and Second (b) generation CT Scanner.....	8
Figure 2.10. Third-generation CT system.....	9
Figure 2.11. Image ring artifacts.....	10
Figure 2.12. Fourth-generation CT scanner.....	10
Figure 2.13. Fifth-generation CT scanner.....	11
Figure 2.14. Sixth generation CT scanner (Helical CT).....	12
Figure 2.15. Slip ring technology.....	12
Figure 2.16. Helical CT Scanner.....	13
Figure 2.17. Multi-Section CT.....	14
Figure 2.18. Digital image process.....	15
Figure 2.19. Small elements of CT images.....	15
Figure 2.20. Interpolation process.....	16
Figure 2.21. 2-Dimensional Radon Transform of the function $f(x, y)$	17
Figure 2.22. Tomographic Reconstruction analytical process.....	18
Figure 2.23. Reconstruction Methods	19
Figure 2.24. Image formation according to the number of projections in SBP.....	20
Figure 2.25. Fourier space by the Slope Function (Ramp filter).....	21
Figure 2.26. Low-Pass filters (Window Function).....	22
Figure 2.27. Schematic view of the IR process.....	22
Figure 2.28. CT Number Ranges in Hounsfield Units.....	25
Figure 2.29. Image Window Width (WW).....	26
Figure 2.30. CT images of Catphan 600 (CTP404) modules for measuring CNR....	31

Figure 2.31. Water phantom for CT number uniformity and noise measurement.....	32
Figure 2.32. A restructured portion of a CATPHAN® phantom.....	33
Figure 3.1. Ion chamber on the center of CTDI phantom.....	35
Figure 3.2. Ion chamber positions on phantom.....	36
Figure 3.3. Cathpan phantom.....	36
Figure 3.4. Aligning Cathpan phantom with internal laser lights.....	37
Figure 3.5. Cathpan 600 phantom (CTP 591).....	39
Figure 3.6. IQ works program for MTF calculation.....	39
Figure 3.7. CTP 404 Module and ImageJ program for CNR measurement.....	39
Figure 3.8. CTP 515 Low contrast module of Cathpan 600 phantom.....	40
Figure 4.1. MTF results for standard filter and 125 mA	43
Figure 4.2. Percentage values of MTF with Standard Filter.....	44
Figure 4.3. MTF results for Detail filter and 125 mA.....	44
Figure 4.4. Percentage values of MTF with Detail Filter.....	45
Figure 4.5. MTF graphs for different mA values and reconstruction filters.....	45
Figure 4.6. MTF graphs for different mA values and ASIR40 reconstruction filters....	46
Figure 4.7. MTF percentage values graphs for different mA	47
Figure 4.8. MTF percentage values graphs for different mA and ASIR40	47
Figure 4.9. MTF percentage values graphs for different slice thickness	48
Figure 4.10. MTF percentage values graphs for different slice thickness and ASIR40.....	48
Figure 4.11. CNR results for standard filter and 125 mA.....	49
Figure 4.12. CNR results for Detail filter and 125 mA.....	50
Figure 4.13. CNR graphs for different mA and reconstruction filters.....	51
Figure 4.14. CNR graphs for different mA and ASIR40 reconstruction filters.....	51
Figure 4.15. CNR graphs for different slice thickness and reconstruction filters.....	52
Figure 4.16. CNR graphs for different slice thickness and ASIR40 reconstruction filters.....	53
Figure 4.17. CNR results for Water in different mA.....	53
Figure 4.18. CNR results for PMP in different mA.....	54
Figure 4.19. CNR results for Teflon in different mA.....	55
Figure 4.20. SNR result for Standard Filter and Detail Filter with FBP.....	55

Figure 4.21.SNR result for different mA and FBP filter.....56
Figure 4.22.SNR result for different mA and ASIR40 reconstruction filter.....57
Figure 4.23.SNR graphs for different slice thickness and FBP filter.....57
Figure 4.24. SNR graphs for different slice thickness and ASIR40 Reconstruction filter.....58



LIST OF SYMBOLS AND ABBREVIATIONS

ASIR	Adaptive Statistical Iterative Reconstruction
AAPM	American Medical Physicians Association
CT	Computed tomography
CTDI	Computed Tomography Dose Index
CAT	Computed Axial Tomography
DLP	Dose Length Product
FBP	Filtered Back-Projection
FOV	Field of View
HU	Hounsfield Units
ICRP	International Commission on Radiological Protection
IR	Iterative Reconstruction
MDCT	Multislice Computed Tomography
PET	Positron Emission Tomography
QA	Quality Assurance
SBP	Simple Back Projection
SPECT	Single Photon Emission Computed Tomography
$CTDI_{vol}$	Volumetric Computed Tomography Dose Index

N : The number of tomographic sections simultaneously displayed in a single-axis axial scan.

T : Single tomographic section width

D_z : Radiation dose profile measured along the z-axis in a single-turn scan.

f : Irradiation factor from irradiation

C : Ion chamber calibration factor

I : 1-turn rotation of the beam tube is the table travel distance.

ABSTRACT

Alcan, E. (2019). Effects of Iterative Reconstruction on Image Quality and Patient Dose in Computed Tomography. Yeditepe University, Institute of Health Science, Department of Health Physics, MSc thesis, İstanbul.

In this thesis, the effects of iterative reconstruction algorithms on image quality and patient dose were investigated. PET / CT tomography device in Yeditepe University Specialized Hospital was used. In the abovementioned system, both unfiltered back projection and iterative reconstruction algorithm can create tomography. Computed tomography dose index (CTDI) values, CTDI phantom, and 10cm pen-type ion chamber were used for different irradiation parameters. Cathpan 600 phantom was chosen for image quality evaluation. Evaluation of image quality parameters (free software) was performed using IMAGE J and IQ WORK software. The irradiation parameters of the tomography system were 120 kVp and chosen three different mA values. CTDI values for these different mA values were measured and compared with the values given by the system. Both 2,5 mm and 5 mm tomographic sections were obtained. Filtered back projection and iterative reconstruction parameters were obtained at 20,40,60,80 and 100 values by using standard and detail filters of Catphan 600 phantom. Image quality parameters such as CNR, SNR, MTF, and homogeneity were evaluated for all reconstruction methods from Catphan 600 phantom images.

Finally, iterative methods can be used to reduce the dose while preserving the image quality and it is also recommended to take the clinic under these conditions.

Different quantitative image quality parameters at different dose levels were evaluated by the CT component of the PET / CT in the Nuclear Medicine Department of Yeditepe University Specialized Hospital besides obtained tomography kept the irradiation conditions low with the same image quality.

Key words: Iterative Reconstruction, Iterative Reconstruction Algorithms, Computed Tomography.

ÖZET

Alcan, E. (2019). Bilgisayarlı Tomografide İteratif Rekonstrüksiyon Algoritmalarının Görüntü Kalitesi ve Hasta Dozu Üzerindeki Etkileri. Yeditepe Üniversitesi Sağlık Bilimleri Enstitüsü, Sağlık Fiziği, Master Tezi. İstanbul.

Bu tez çalışmasında bilgisayarlı tomografide iteratif rekonstrüksiyon algoritmalarının görüntü kalitesi ve hasta dozu üzerindeki etkileri incelenmiştir. Çalışmamızda Yeditepe Üniversitesi İhtisas Hastanesindeki PET/CT tomografi cihazı kullanılmıştır. Bu sistemde hem filtrelenmemiş geriye projeksiyon hem de İteratif Rekonstrüksiyon algoritmasıyla tomografi oluşturma olanağı bulunmaktadır. Farklı ışınlama parametrelerinde bilgisayarlı tomografi doz indeksi (CTDI) değerleri, CTDI fantomu ve 10cm uzunluğunda kalem tipi iyon odası kullanılmıştır. Görüntü kalitesi değerlendirmesi için Cathpan 600 fantomu kullanılmıştır. Görüntü kalite parametrelerinin değerlendirmeleri ücretsiz yazılımlardan olan IMAGE J ve IQ WORK yazılımları kullanılarak gerçekleştirilmiştir. Tomografi sistemi ışınlama parametreleri 120 kVp ve üç farklı mA değerinde yapılmıştır. Bu farklı mA değerleri için CTDI değerleri ölçülerek ve sistemin verdiği değerler ile karşılaştırılmıştır. Hem 2,5 mm hem de 5mm tomografik kesitler elde edilmiştir. Catphan 600 fantomuna ait standard ve detay filtreleri kullanılarak filtrelenmiş geriye projeksiyon ve iteratif rekonstrüksiyon parametreleri 20, 40, 60, 80 ve 100 değerlerinde kullanılarak iteratif olarak elde edilmiştir. Catphan 600 fantomu görüntülerinden tüm Rekonstrüksiyon yöntemleri için CNR, SNR, MTF ve Homogeneity gibi görüntü kalitesi parametreleri değerlendirilmiştir.

Son olarak görüntü kalitesini koruyarak iteratif yöntemlerle doz azaltılabileceği belirlenerek ve kliniğe bu şartlarda çekim yapılması önerilmiştir. Yeditepe Üniversitesi İhtisas Hastanesi Nükleer Tıp kliniğinde bulunan PET/CT cihazının CT komponentinde farklı doz seviyelerinde kantatif görüntü kalitesi parametreleri değerlendirilerek aynı görüntü kalitesinde daha düşük ışınlama şartlarında tomografinin çekilmesi sağlanmıştır.

Anahtar Kelimeler: İteratif Rekonstrüksiyon, Bilgisayarlı Tomografide İteratif Rekonstrüksiyon Algoritmaları, Bilgisayarlı Tomografi.

1.INTRODUCTION

Computed Tomography (CT) is a radiological imaging method that produces transverse tomographic images with high accuracy of x-ray attenuation in the examined part. The mathematical basis of computed tomography was developed in 1917 by Radon. Radon proved that the object could be reconstructed using an infinite number of cross-sectional image information around an object. The first tomography was developed in 1972 by Godfrey Hounsfield and Allan Cormack. They were awarded the Nobel Prize for their achievements.

In Computed Tomography, a large number of two-dimensional images of an object are taken from different angles using an X-ray, and a three-dimensional image of the internal structure of this object is obtained. In CT, X-rays coming out of the tube are diverted into a thin beam by a process called collimation. The collimated X-rays are detected by detectors after passing through the body of the patient and the attenuation of the rays is determined. The determined attenuation coefficients are then used for the generation of the image.

The tomographic reconstruction method is used for image formation. When tomographic reconstruction collects a series of measurements, each measurement is the sum of the attenuation coefficients of the object along a given beam path. These measurements are collected from different angles and at different distances from the isocenter. These measurements form a "view" or "projection".

Multi Slice Computed Tomography (MSCT), a groundbreaking development in computed tomography practice, has led to major advances in CT technology. After 1989, helical scanning was developed and devices were produced in 1991, which can take sections less than 1 mm. In the same year, the forerunner of today's MSCT technology, twin-detector helical CT was developed.

In this commonly preferred diagnostic method, it is important to reduce the patient dose to the lowest dose possible while maintaining the same image quality. In recent years, it has become possible to obtain high quality tomography under low irradiation conditions and therefore at low doses with the emergence of iterative techniques. As it is seen in many studies, the iterative techniques provide the same quality images with less patient dose (1).

In this study, it was aimed to obtain images with image quality phantom of CT in Yeditepe University Hospital Nuclear Medicine Department and to evaluate the dose reduction and image quality parameters by applying different reconstruction algorithms.



2.GENERAL INFORMATION

2.1.History of Computed Tomography

In 1917, Bohemian mathematician Radon proved that if integral values were known along any number of lines passing through the same layer, this integral distribution could be calculated. The first experiment in the medical applications of reconstructive tomography was performed by physicist A M Cormack. Between 1957 and 1963 he developed a method for calculating radiation absorption distributions based on transmission measurements in the human body. He indicated that for radiological applications, it could be possible to show the slightest differences in attenuation, even different soft tissue structures. In 1963, Kuhl and Edwards introduced the concepts of emission computed tomography. In 1967, filtered back-projection was first described by Bracewell and Riddle. In 1970, explanations of algebraic reconstruction techniques were described by Gordon et al. In 1971, Bates and Peters Fourier described the reconstruction techniques. The first successful practical application of the theory was carried out in 1972 by British engineer G N Hounsfield. In 1979, Hounsfield and Cormack received the Nobel Prize in Medicine for their achievements (2).

Table 2.1. Summary of CT History

1917	Radon	Mathematical basis of computed tomography.
1957	A M Cormack	First experiments on medical applications
1963	A M Cormack	Developed a method for calculating radiation absorption distributions.
1963	Kuhl and Edwards	Concepts of emission computed tomography
1967	Bracewell and Riddle	Filtered back projection
1970	Gordon et al	Explanations of algebraic reconstruction techniques
1971	Bates and Peters	Fourier reconstruction techniques
1972	G N Hounsfield	The first successful practical application of CT

2.2. General Principle of Computed Tomography

Computed tomography (CT) is a radiological imaging system that determines the distribution of x-ray attenuation in the examined section and produces transverse tomographic images as shown in figure 2.1 (1).

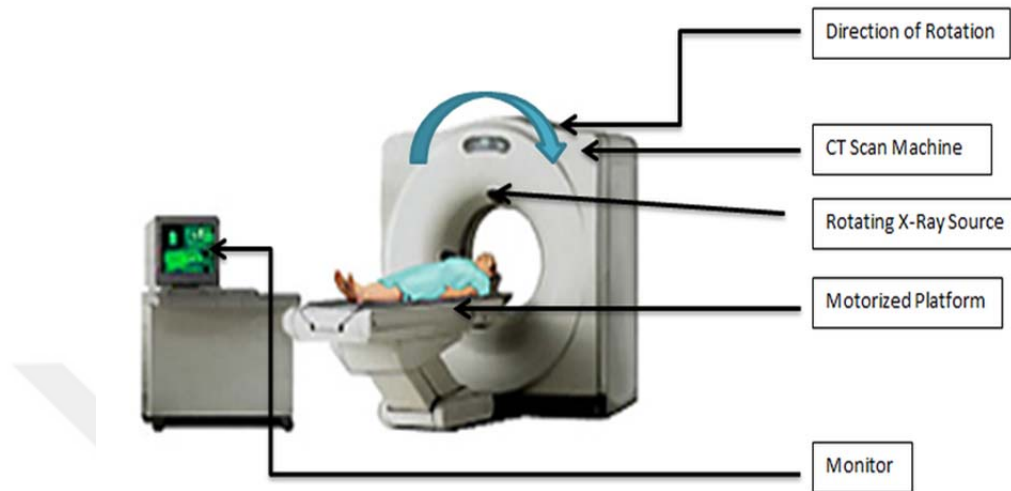


Figure 2.1. Computed Tomography

A collimated high kilovolt X-ray as shown in figure 2.2 passes through the tissues of the patient and the rays attenuated by the patient are detected. The attenuation coefficients of the beam emitted from the X-ray tube are determined by this method.

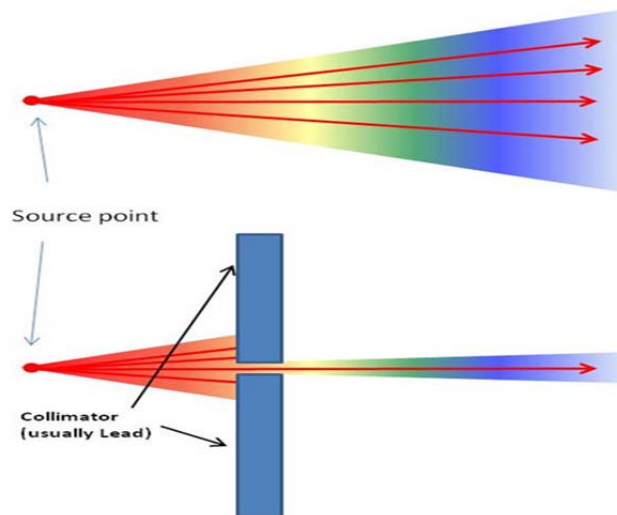


Figure 2.2. Collimated Beam

Similar to the conventional radiography as shown in figure 2.3, the X-ray intensity behind the object is measured to create a projection image. A single transmission measurement performed by a detector at a given moment is called a beam. The series of rays in the same direction are called projections (3).

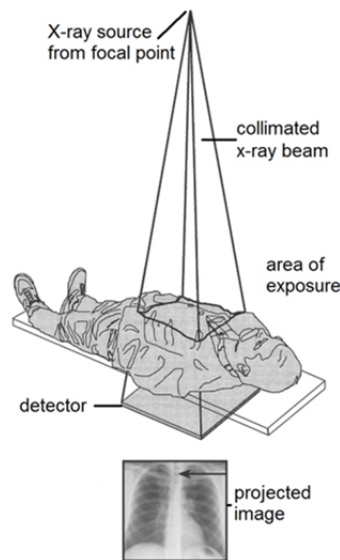


Figure 2.3. Creation CT projected image

Two types of projection geometry are used in CT imaging as shown in figure 2.4: parallel beam and fan-beam geometry. In parallel beam geometry, all rays in a projection are parallel to each other. In fan-beam geometry, the rays in a projection are inclined.

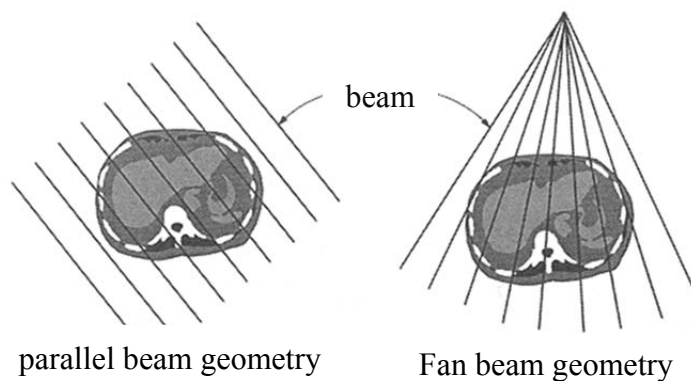


Figure 2.4. CT Projection Geometry

The attenuation value is calculated from the source to the detector along each beam by measuring the intensity of the rays outgoing from the X-ray tube and comparing it to the attenuated beam as shown in figure 2.5. These values are directly proportional to the coefficient of linear attenuation of the tissues through which the beam passes and the thickness of the object.

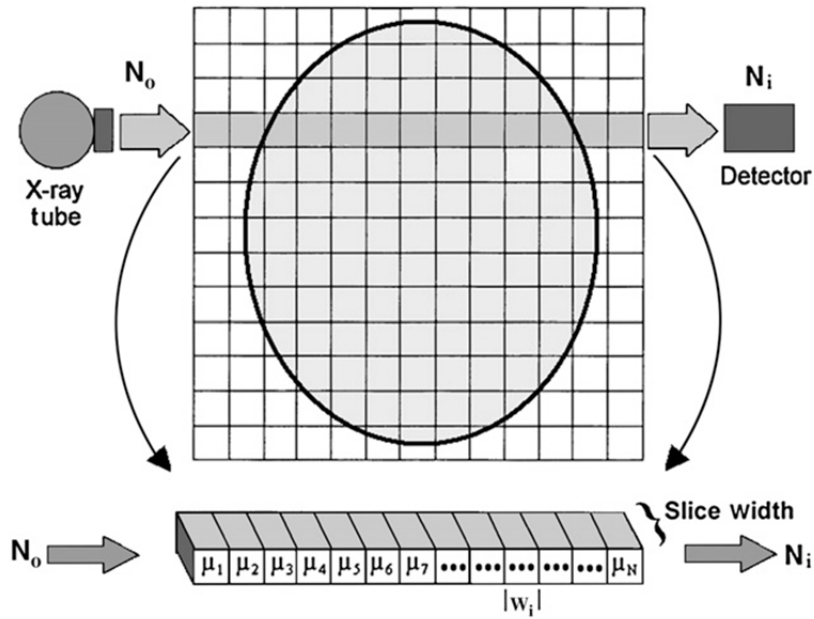


Figure 2.5. Attenuated Coefficient of X-ray beam

$$N_i = N_0 e^{-\mu x} \quad (2.1)$$

$$\ln\left(\frac{N_0}{N_i}\right) = \mu x \quad (2.2)$$

According to beer Lambert law (the attenuation of the x-rays can be written with this formula) as in equations 2.1 and 2.2, only one projection is not enough to calculate the slice image of the patient in CT as in figure 2.5. In equation 2.1, N_0 value can be taken from the air calibration of CT. The air calibration can be done without an object in the gantry. N_i value is measured when the patient is located in the gantry. However, in one line five hundred twelve unknown new values are measured. For another ray five hundred twelve unknown new values can also be measured. So in one slice five hundred twelve times five hundred twelve (512x512) unknown new values are obtained.

Rotation of gantry is required to calculate these values. And other projections such as other equations with unknown values must be taken. About one thousand projection images are obtained for a patient at the end of the imaging session. So eight hundred thousand equations are obtained to be solved.

Attenuation data from different projections are recalculated using a mathematical process called Image Reconstruction as shown in figure 2.6.

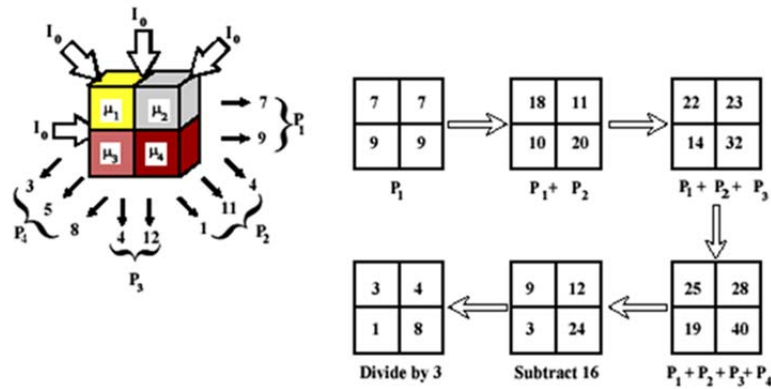


Figure 2.6. Mathematical process of Image Reconstruction.

This produces a matrix of average relative X-ray absorptions in each volume element (voxel) of the matrix in the tissue slice examined (4).

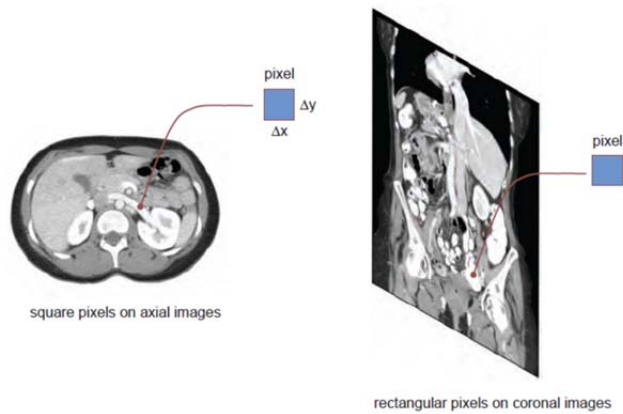


Figure 2.7. Pixels on CT images.

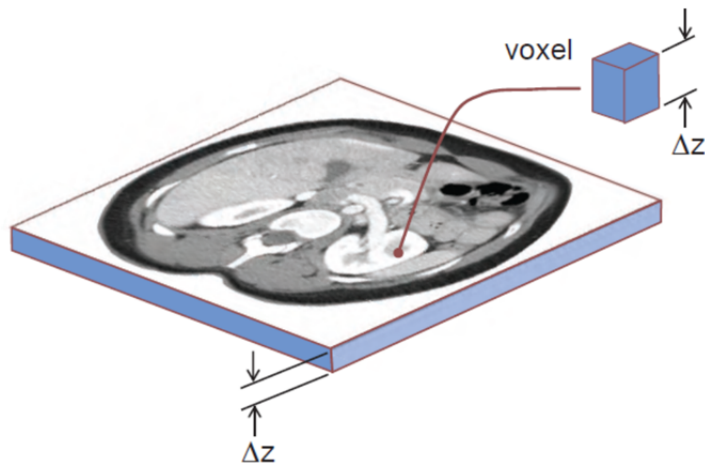


Figure 2.8. Voxel on CT images.

A pixel as shown in figure 2.7 represents a two-dimensional image of a three-dimensional voxel as shown in figure 2.8 within the object; the third dimension is the slice thickness of the examined section.

Over time different generation scanners have been developed. The first generation scanners had an X-ray tube that produced a pen-shaped beam that fell on a single detector (3). A narrow pen width X-ray and a single detector mechanism were used for data collection. Scanning was performed in rotate-translate motion. The X-ray tube and single detector were scanning the patient from one end to the other.

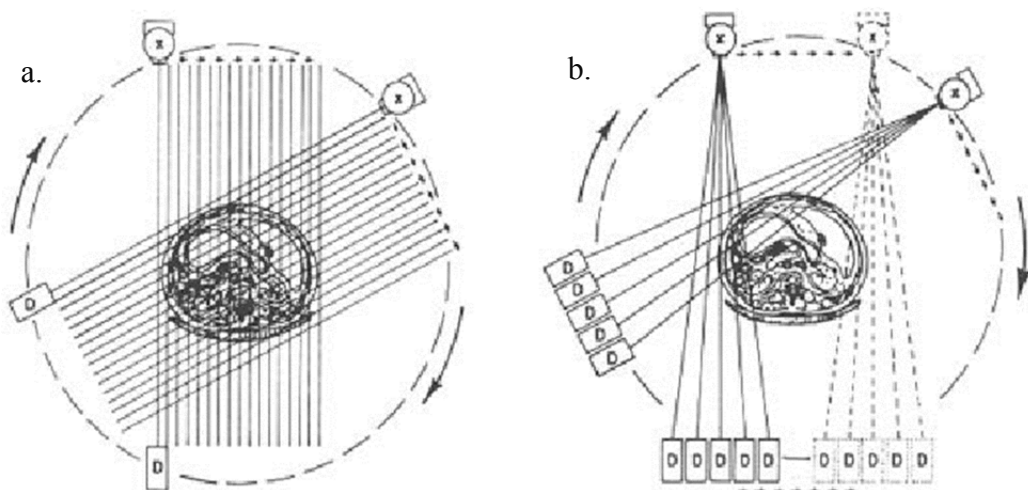


Figure 2.9. First (a) and Second (b) generation CT Scanner

The first generation CT scanners performed an axial scan as shown in figure 2.9 in part a. The X-ray tube was not always open. The patient table was fixed but the x-ray tube was active. When the system received 360-degree projection data, the tube was deactivated. As shown in figure 2.9 in part b, the second-generation CT scanners had a narrow fan beam that fell into a small array of curved detectors. Today, the most widely used systems are third-generation systems as shown in figure 2.10. Fan-beam shaped X-ray collimation is used. The X-ray passing through the patient falls into the Xenon gas-filled or solid-state scintillation detectors. The detector and the X-ray tube move differently from the first and the second generation. They have multiple detector arrays and scan time is as fast as 0.5 seconds per turn or per slice (5).

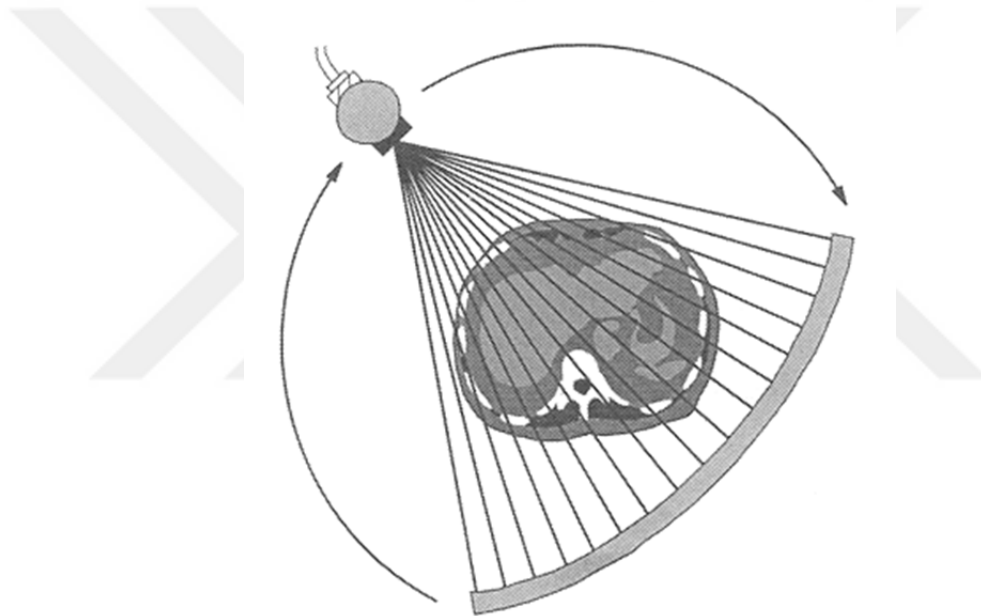


Figure 2.10. Third-generation CT scanner

Each detector forms a ring in the image in the third generation CT scanners. Over time, deviations in the signal levels of the detectors affected the attenuation values. These reduction values make up the image that causes the ring artifacts as shown in figure 2.11.

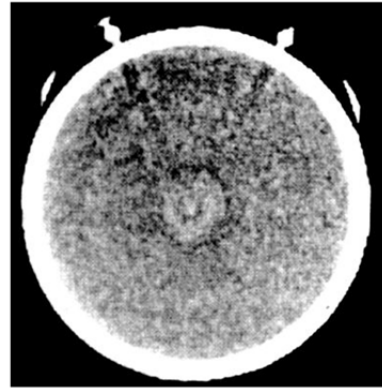
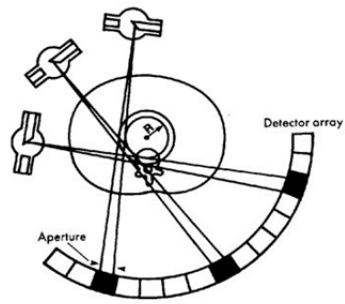


Figure 2.11. Image ring artifacts

In the fourth generation, as shown in figure 2.12, there are static detectors in the form of a circle in the portal. In these systems, only the X-ray tube moves. They have a fixed ring of detectors with approximately 4800 detectors and only the X-ray tube rotates around the patient. These generation CT scanners are designed to eliminate the ring artifact. This method is more expensive than the others because of the number of detectors. This system was quickly abandoned.

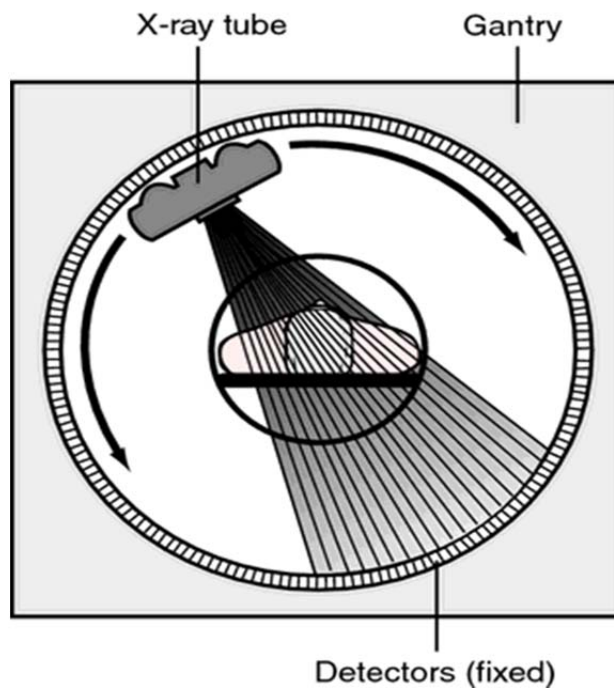


Figure 2.12. Fourth-generation CT scanner

The fifth-generation as shown in figure 2.13, CT was developed specifically for cardiac tomographic imaging. It does not contain a conventional x-ray tube. A large tungsten arc surrounding the patient was placed at the opposite of the detector ring. The electron beam is directed around the patient to the annular tungsten target. It has a scanning speed of 0.05 seconds (5). It has a rotating electron beam and a fixed tungsten target ring. Electrons from the gun are converted to x-rays by hitting a target, so the produced x-ray is directed to the patient. Because of the high price of the system, it not conventionally used at the moment in Turkey.

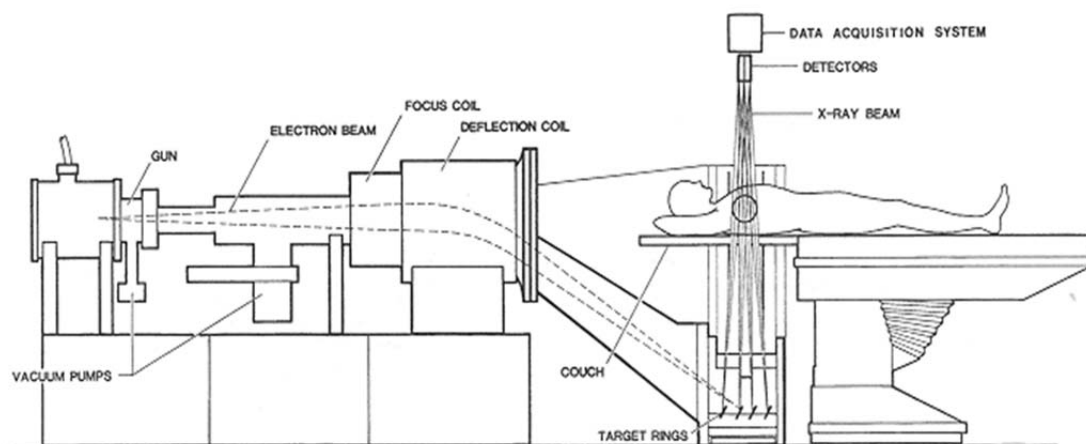


Figure 2.13. Fifth-generation CT scanner

Sixth generation CT, in other words, Helical CT is shown in figure 2.14. Helical CT scanners collect information during the patient's bed is in motion. The total scanning time was considerably shortened by subtracting the time required for the patient bed movement.

It's actually a third-generation CT system with continuous rotation of gantry at the same time as the table moment. In the third generation tomography, the gantry must go back after one turn because of the embrangled cables. Thanks to the slipping technology to make the helical scanning possible.

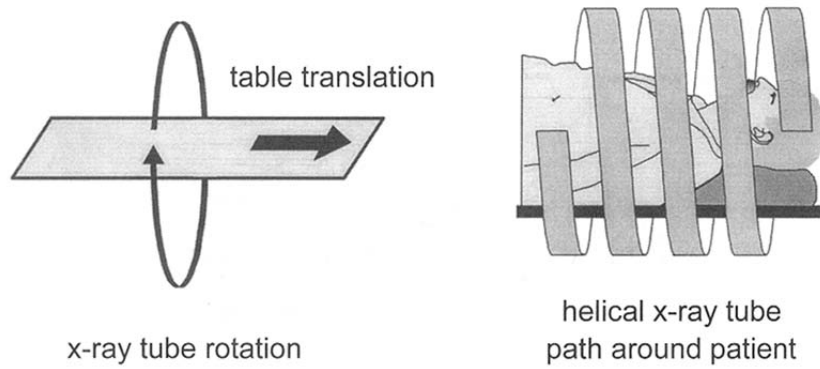


Figure 2.14. Sixth generation CT scanner (Helical CT)

All CT scanners (except generation 4 and 5) require winding and unwinding of connection cables that cause scan delays. The slip ring is designed to eliminate this problem. Slip ring technology is used to transmit data, current or signals from a fixed surface to a rotating surface. In the slipring technology, instead of rotating cables, some brushes touch the ring and the contact signals and current are transmitted into the gantry or outside of the gantry as shown in figure 2.15.

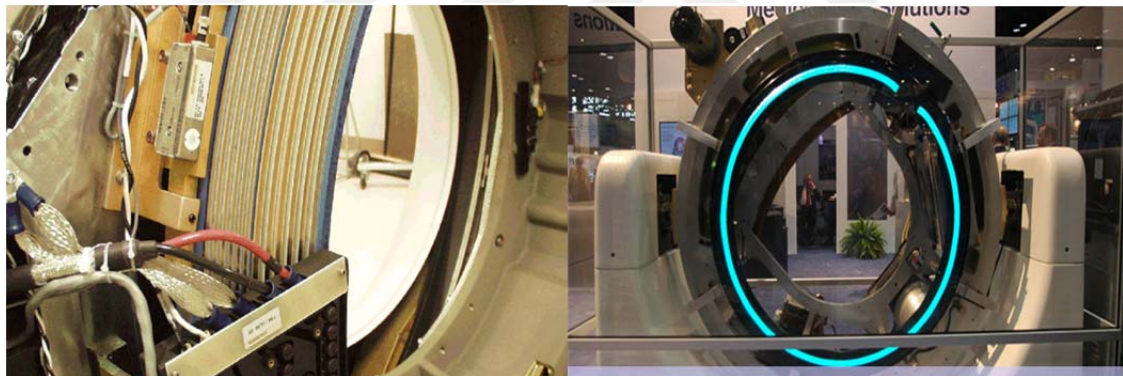


Figure 2.15. Slip ring technology

Data and current transmission are important in diagnostic technology. The advantage of helical scanning is the speed by eliminating the start / stop movement of the table as in the axial CT.

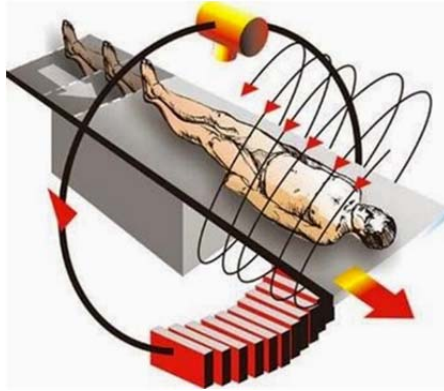


Figure 2.16. Helical CT Scanner

Helical scanning has a pitch factor. The pitch describes the relative progression of the CT table per rotation of the gantry. Pitch expression of helical scan is shown in equation 2.3.

$$pitch = \frac{\text{table travel distance}}{\text{number of slice} \times \text{width of slice}} \quad (2.3)$$

Seventh generation CT: Multi-Section CT (MSCT). When using a multi-section detector array, the collimator aperture is larger than others as shown in figure 2.17 and a large proportion of the x-rays produced from the tube are used for the generation of the image. In single-slice tomography, the collimator aperture increases the cross-sectional thickness and disrupts the separation force in the z-axis direction. In MSCT systems, section thickness is determined by detector size, not by collimator.

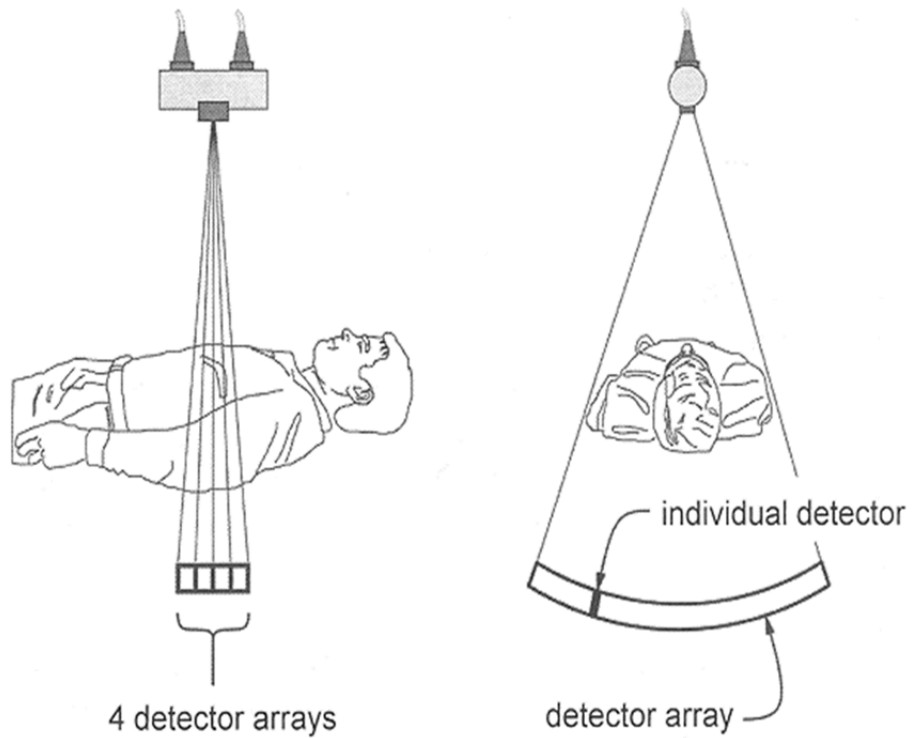


Figure 2.17. Multi-Section CT

Table 2.2. Generations of CT (summary)

1st Generation CT	Axial Scan, pen-beam, single detector, the X-ray tube is not always open
2nd Generation CT	Axial Scan narrow fan beam, curved detectors
3rd Generation CT	Broom-shaped, continuously rotatable tubes, multiple detector arrays
4th Generation CT	Static detectors, form of a circle in the portal, X-ray tube moves
5th Generation CT	Electron beam, tungsten target, detector ring
6th Generation CT	Helical Scan, patient bed movement
7th Generation CT	Multi-Section CT, multi-section detectors

2.3. Image Reconstruction on Computed Tomography

The process of using measured projection data to create a tomographic image is called tomographic reconstruction as shown in figure 2.18.

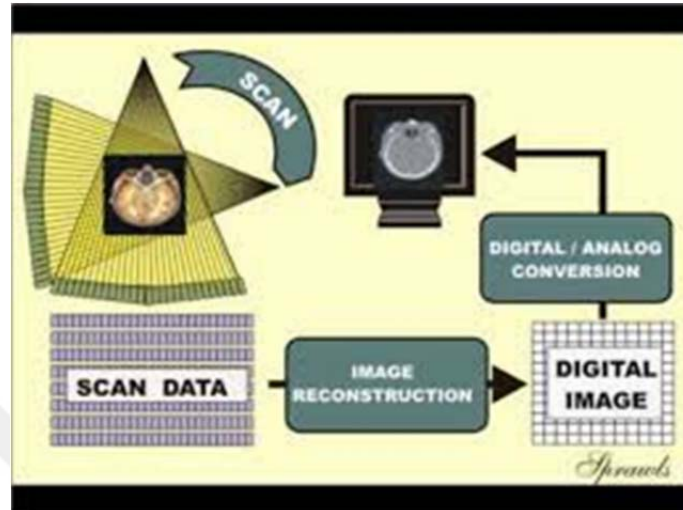


Figure 2.18. Digital image process

As for all digital images, the image in CT consists of small elements (pixels). This is called the image matrix. The number of matrices is shown as the multiplication of the number of pixels on both sides of the image, and in current devices, this number is usually 512x512.

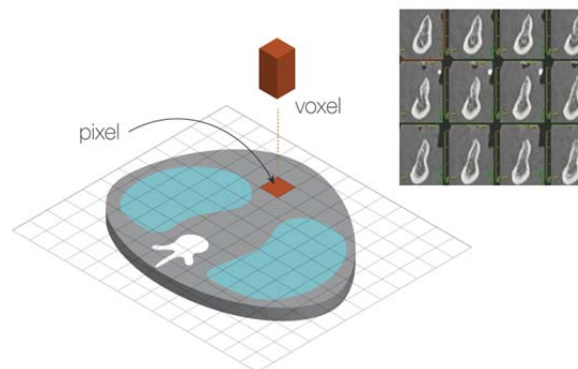


Figure 2.19. Small elements of CT images

Tomographic reconstruction is the sum of the attenuation coefficients of the object along a certain beam path of each series of measurements. These measurements are collected at different angles and at different distances from the isocenter (6). First, a series of measurements are performed along the properly separated parallel paths. These measurements create a ‘view’ or ‘projection’. The same measurement process is then repeated at a slightly different angle. This process continues until 360 degrees (theoretically only 180 degrees of projection is required in parallel) is covered. During the entire process, the angular increase between adjacent views and the scanned object remains constant (1).

CT image algorithms assume that the x-ray source moves around the patient in a circular (not helical) direction. Prior to the section image, the helical data sets are interpolated as shown in figure 2.20 into a series of planar data sets. Interpolation is a mathematical process used to smooth, enlarge or average images that are being displayed with more pixels than that for which they were originally reconstructed.

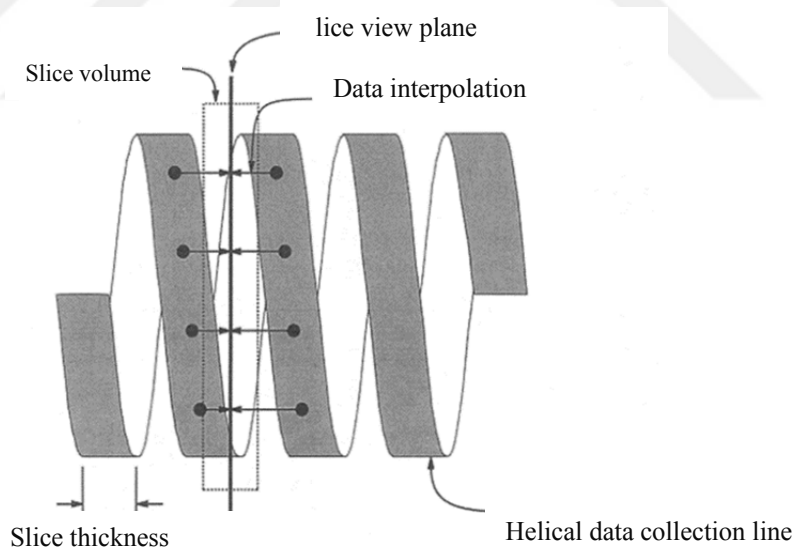


Figure 2.20. Interpolation process

The Radon transform is mostly applied in image reconstruction. The projections are commonly generated by cross-sectional scans of the object. The Radon transform creates the objects by integrating a function as shown in figure 2.21, called indicator or

characteristic function, over straight lines. In computed tomography scans, the indicator function is the attenuation coefficient's function.

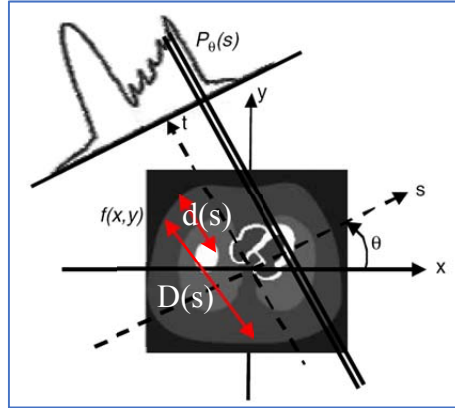


Figure 2.21. 2-Dimensional Radon Transform of the function $f(x, y)$.

$$P_{\theta}(s) = \int_{D(s)} f(s, t) dt = \iint_{-\infty}^{\infty} f(x, y) \delta(x \cos \theta + y \sin \theta - s) dx dy \quad (2.4)$$

$$s = x \cos \theta + y \sin \theta \quad (2.5)$$

$$t = -x \sin \theta + y \cos \theta \quad (2.6)$$

As shown in equation 2.4, this expression is called the 2-Dimensional Radon Transform of the function $f(x, y)$. If a 2-D Inverse Radon Transform of 1-D projections is taken, a 2-D cross-sectional view of the object is obtained.

Analytically, projection information is obtained and the sets of equations are generated with this information as shown in figure 2.22. After the solution of these equations, a cross-sectional view is received.

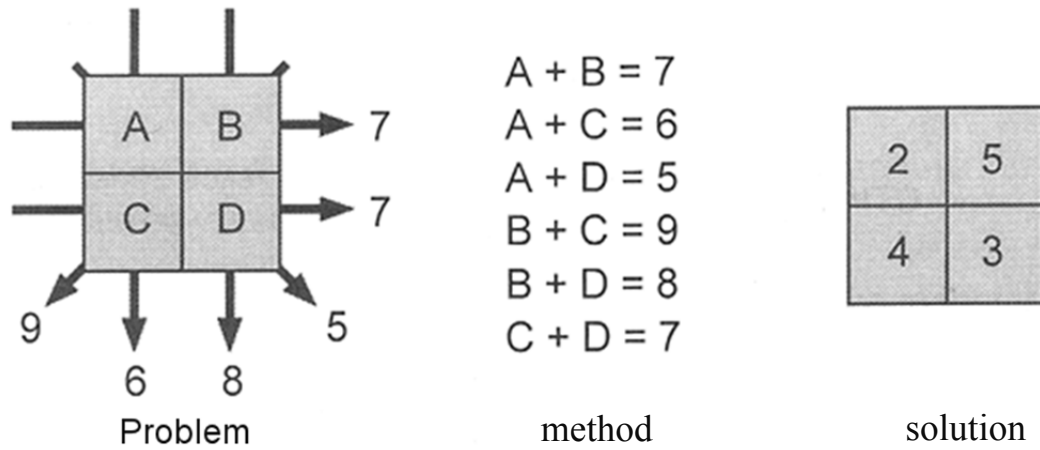


Figure 2.22. Tomographic Reconstruction analytical process

A standard tomography uses approximately one thousand projections to create a cross-section and 800 equations per projection and that is, about 800 thousand sets of equations. The unknown number is about 512 thousand in a 512×512 standard CT image. This is a very time-consuming process, so techniques should be developed for these calculations to be done in a short time. Like SBP, FBP, and IR (1) many reconstruction methods techniques have been improved for these calculations. It can be classified as two groups as shown in Figure 2.23.

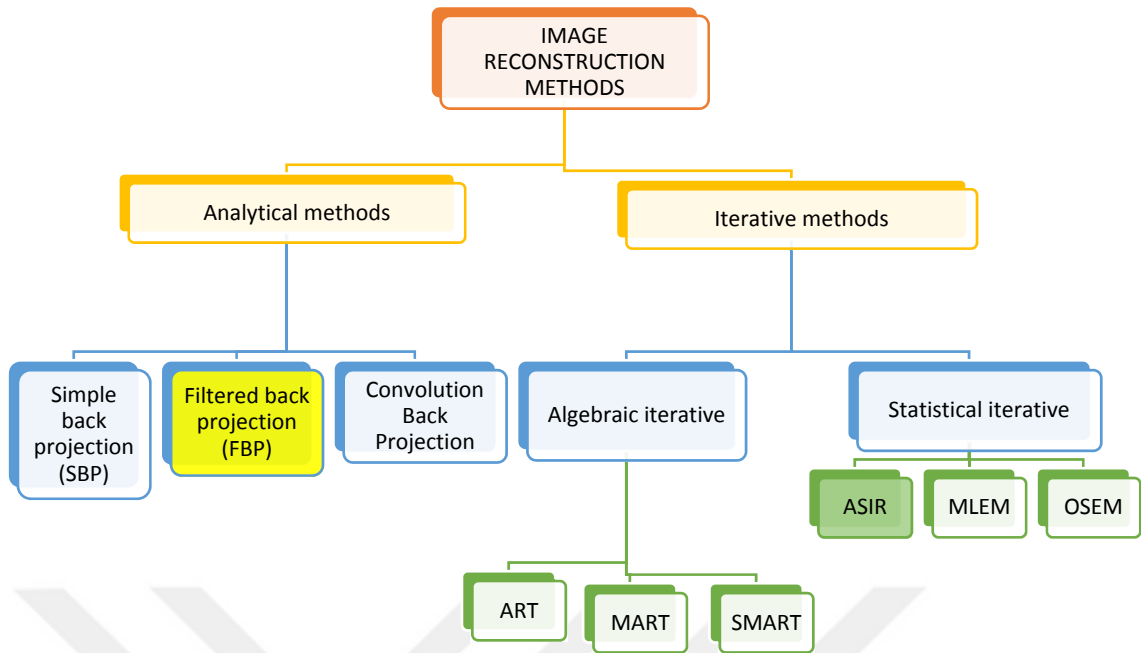


Figure 2.23. Reconstruction Methods

Image reconstruction methods are divided into analytical and Iterative. One of the most widely used analytical methods is Filtered Back Projection (FBP).

2.3.1. Simple Back Projection

The process of converting the data from the projection profile to a matrix is known as back projection. Each projection obtained in the Simple Back Projection method is projected back to the pixels in the cross-sectional image matrix generated computationally at the same angle. This projection is applied to all pixels that correspond to a point in the projection, as the projections do not have depth information (7).

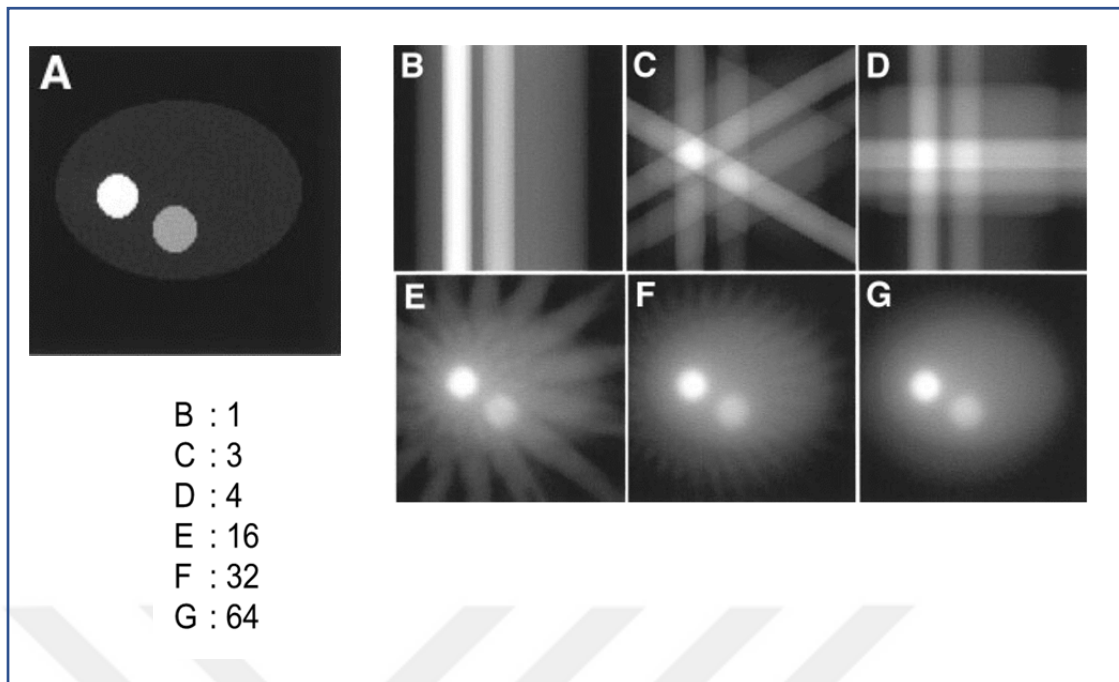


Figure 2.24. Image formation according to the number of projections in SBP.

As shown in figure 2.24, it belongs to the actual image in A. The image in B is the x-ray absorption of these two objects according to a projection taken from one angle. Since the depth of these objects cannot be known, they are projected back that they can be at all depths in that direction. This is the reason for the line in the image. If a simple back-projection is made with one projection information, it doesn't give the real information. The image obtained using with three different projection angles is shown in Figure 2.23 C. When the information obtained from four, sixteen, thirty-two and sixty-four projections are projected back, the formed images are illustrated in D, E, F and G. As the number of projections used increases, the actual image becomes relatively clear. But a blur effect is also observed. Filtered back projection is preferred to remove this blurring.

2.3.2. Filtered Back-Projection (FBP)

Filtered back projection is an analytic reconstruction algorithm designed to overcome the limitations of conventional back-projection. It applies a convolution filter to remove

blurring. Convolution is the mathematical property that describes the blurring process in medical imaging. This algorithm consists of ramp filtering and back projection procedures. Ramp filtering can be implemented as a convolution in the spatial domain or multiplication in the Fourier domain.

$$f_B(x, y) = F_{2D}^{-1} \left(\frac{F(v_x, v_y)}{|v_r|} \right) \quad (2.7)$$

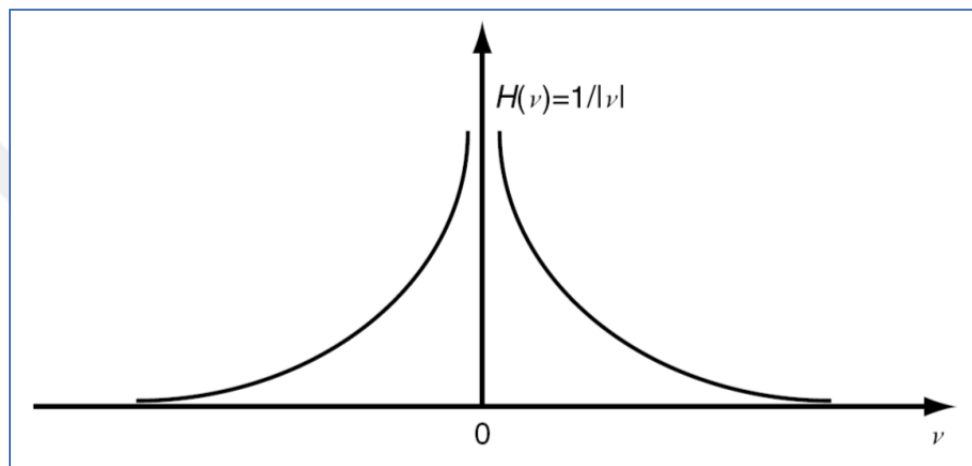


Figure 2.25. Fourier space by the Slope Function (Ramp filter)

In this method, the projected image is multiplied by the Slope Function (Ramp filter) in the Fourier space and then the inverse Fourier Transform is applied as shown in equation 2.7. The ramp function increases the amplitude of the high-frequency noise. For this reason, Low-Pass filters (Window Function) are used as shown in figure 2.26. These filters reduce the amplitude of the high-frequency information (7).

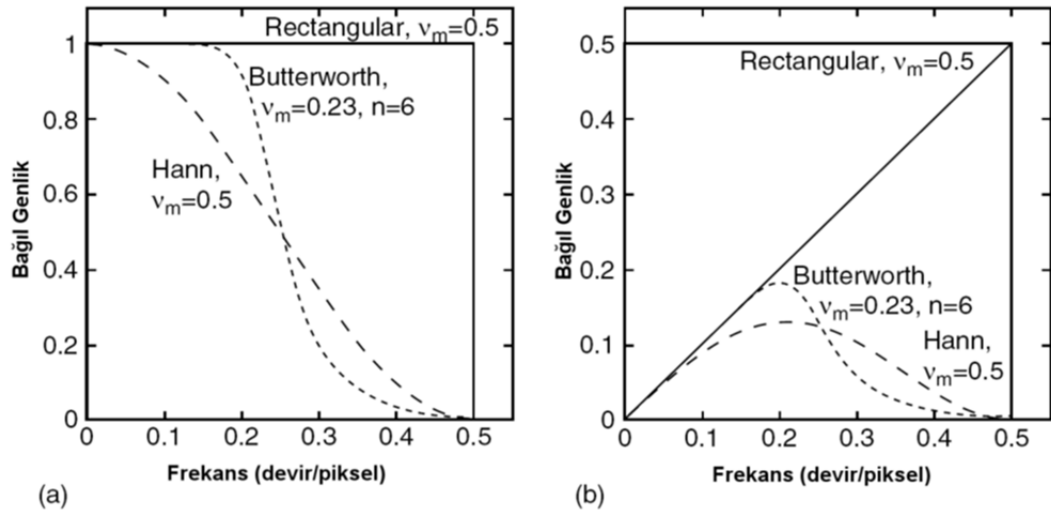


Figure 2.26. Low-Pass filters (Window Function)

2.3.3. Iterative Reconstruction (IR)

Iterative reconstruction (IR) is an alternative image reconstruction method allowing to get images at lower radiation doses with similar noise levels and similar image quality compared to routine dose with FBP. IR techniques go through a series of repetitions during the CT reconstruction process. The first image may start as an estimation of a fixed image, or an FBP image (7).

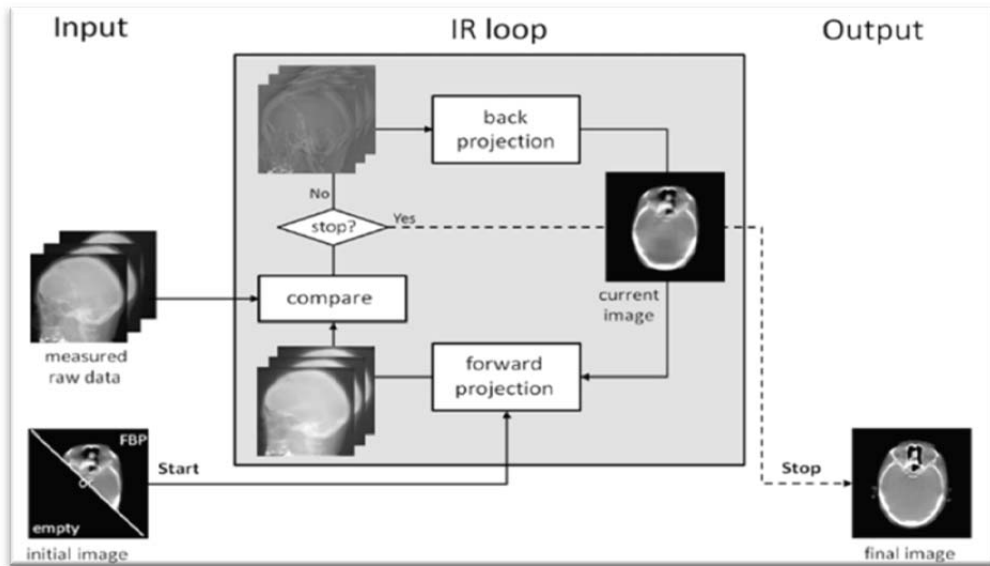


Figure 2.27. Schematic view of the IR process.

As shown in figure 2.27, Firstly, it starts with an initial image. Forward projection is applied to the initial image and it is compared with measured raw data. If the difference between them is low enough, the process is stopped. If not enough, it is back-projected to obtain the current image. Until the necessary differences are found, the system stops and gives a real reconstruction image. If not, process continuous.

IR is a mathematical algorithm that provides image formation with less radiation dose in similar noise and image quality compared to FBP (8). In other words, it is a dose reduction method without changing the image quality (9). IR is a numerically complex and dense algorithm. Projection data are used to reconstruct, but if the CT image is known, projection data can be calculated using forward projection. IR techniques go through a series of repetitions during the CT reconstruction process. The IR then makes the update that allows the image of the scanned object to be displayed correctly (3).

An IR noise reduction algorithm can be used for two main purposes. To increase the quality of an image at the same radiation dose and to reduce radiation dose without changing image quality (10). Along with the IR technique, it is necessary to optimize the other parameters used to reduce the dose of CT. These are similar parameters such as tube current, voltage current and section thickness (11).

Advantages of Iterative Methods; The biggest limitation in analytical algorithms is the physical effects such as noise and photon reduction not being reflected in the algorithm. In iterative methods, noise can be directly modeled in the algorithm. In addition, iterative methods are suitable to solve complex physical models of emission and detection problems, such as position-related reduction coefficients and distance-dependent separation power.

Disadvantages of Iterative Methods; The main disadvantage of the iterative algorithms is the longer computing time. However, advances in computer technology and some acceleration methods have made iterative techniques a clinically usable method (3).

There are many iterative reconstruction methods. One of them is the ART(Algebraic Reconstruction Technique) (12). The ART method starts with an initial image estimation as in all of the iterative methods. The projections are calculated using the forward projection from the initial image. The initial image is modified by a difference that compensates for the difference between measured and calculated projections. Once the correction factors for the projection at an angle are calculated, the

factors are reflected in the pixel values. These new values are taken as initial images for the next projection. When the update is complete for all projections, iteration is completed.

There remain variants in the ART Method. Because the correction methods are applied as a multiplication technique, it is known as MART (Multiplative ART). AART (Additive ART) is another variant. Corrections to the simultaneous repetition of the image (SIRT, Simultaneously Iterative Reconstruction Technique) are made concurrently after all projections are completed, not after each projection. The SMART method, which is a combination of MARM and SIRT, produces clinically more successful images than both methods. In the block iterative version of the ART method (BI-ART), multiple projections are grouped and corrected (12).

With a relatively low number of counts in nuclear medicine, the information gathered is high with statistical methods. It is impossible to remove the actual solution from this type of data and therefore it gives the best solution. The best solution in statistical methods is defined as the most likely solution from the data (12).

Although there are many approaches in determining the Maximum Probability (ML), the most commonly used is Expectation-Maximization (EM). The EM algorithm consists of two independent steps: In the first step, projections are estimated by the forward projection method using the appropriate system/transition matrix based on the estimated distribution of activity from previous iteration. In the second step, the current estimate is updated so that the probability is maximized by multiplying the difference between the projections measured and the previous estimate (12). In addition, there are many other outstanding features of the algorithm in theory, but the high noise level in emission tomography makes these advantages clinically insignificant. The sequential Sub-Groups EM (OS-EM) method; is an algorithm developed to speed up the ML-EM method. The algorithm is accelerated by making the totals in the ML-EM algorithm through sub-groups selected by the user, not through all projections at once. The image obtained from each subset of iterations with the OS-EM method is almost identical to that obtained from a complete ML-EM iteration unless the number of sub-groups is selected too small. Calculation times are almost the same. Thus, if the number of sub-groups 4 is selected for 128 projections, the OS-EM algorithm runs 32 times faster than

the ML-EM algorithm. In practice, selecting the number of sub-groups 4 provides a good balance between calculation speed and image quality (12).

2.3.3.1. ASIR (Adaptive Statistical Iterative Reconstruction)

It is an iterative reconstruction algorithm that uses FBP images as initial information. In the algorithm, it depends on the user to determine the percentage of iterative information reflected in the image. ASIR is the most comprehensive IR technique. In general, it has been observed that noise is reduced, CNR and SNR values and image quality are improved with this algorithm. (13). The ASIR algorithm determines the noise from the image and then extracts it. To prevent artificially over-magnification of images unfamiliar with radiologists, ASIR allows IR images to be blended with FBP images ranging from 0% ASIR to 100% ASIR (14). Vendors of these algorithms generally recommend the use of 30-50% ASIR, indicating that using this range can reduce the patient dose by 40% (15).

2.4. Hounsfield Unit Scale (windowing) on Computed Tomography

CT numbers characterize the tissue attenuation coefficients in each volume element. The attenuation coefficients obtained from the projection information is expressed as an integer and called the HU value. HU is μ value normalized to μ value of water.

CT numbers range from -1,000 to +3,000:

- 1,000 air
- 300 to 100 soft tissues
- 0 water
- +1,000 to +3,000 bone and contrast agent

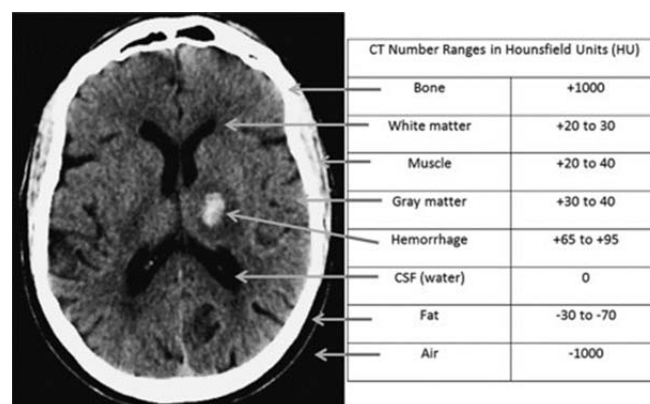


Figure 2.28. CT Number Ranges in Hounsfield Units

CT has a superior tissue contrast. There are different HU values for black, white and different shades of gray to display images. The human eye can only distinguish between 20-30 different gray levels. The window width (WW) corresponds to the HU range represented by the grayscale as shown in figure 2.29, while the window level (WL) defines the central gray color and must be set at the tissue level of interest (3).

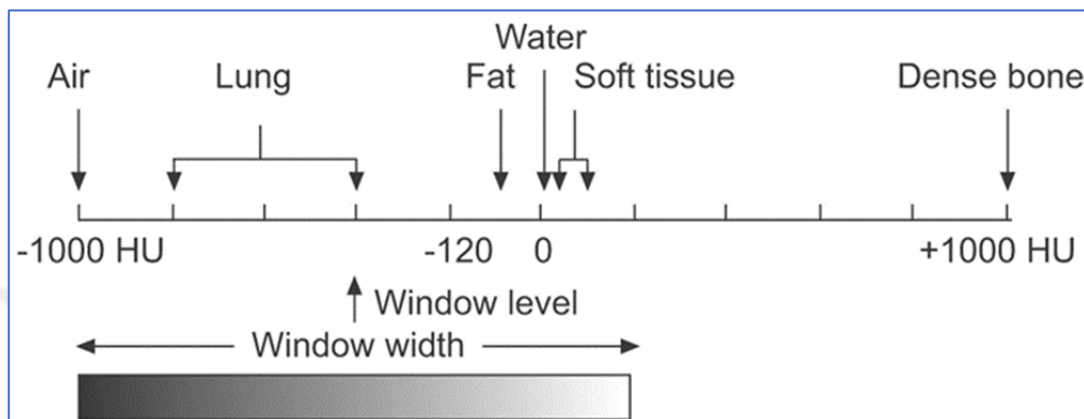


Figure 2.29. Image Window Width (WW)

4096 gray color in a CT image is impossible to detect. Since the difference between grayscale values of gray and white matter in the brain is less than 45 HU, it will not be possible to separate gray matter and white ore in such an image. In order to show this distinction, it is essential to distribute the values of the grayscale in a narrow space where the values of the brain tissue are displayed. This process is called windowing (3). In the CT section of the chest, the mediastinal structures are displayed in the soft tissue window and the lungs in the parenchyma window.

2.5.Dosimetric Parameters in Computed Tomography

In 1981, Shope et al.developed a method to determine the doses given by computed tomography. They presented a CT dose index (CTDI) as a metric to measure radiation output in CT examinations. It is the parameter used to define the radiation dose in computed tomography. The word 'index' is especially added to the name of the CTDI to distinguish the amount of patient dose (16).

2.5.1. Computed Tomography Dose Index (CTDI)

CTDI is the most important dose indicator in the computed tomography. As a result of the irradiation of a section, the doses taken directly from the sections due to scattering are added to the dose taken by that section and expressed as CTDI. A single cross-section in the center of the volume scanned along a series of irradiation sections adjacent to one another is a quantity used to calculate the average dose. CTDI is measured for a single scan in axial scanning mode in the direction parallel to the patient's long axis (z-axis direction). The use of a 3 cc, 100 mm long ion chamber for this procedure is considered to standard. The mathematically most basic form of the CTDI calculated by dividing the value read from the electrometer by the nominal total beam collimation is as follows and the unit is mGy (1).

$$CTDI = \frac{1}{N \times T} \int_{-\infty}^{\infty} D_z d_z \quad (2.8)$$

N: The number of tomographic slices simultaneously displayed in a single-axis axial scan.

T: Single tomographic slice width

D_z : Radiation dose profile measured along the z-axis in a single-turn scan.

Equation for measurement with ion chamber with active length L is written as follows:

$$CTDI_L = \frac{1}{N \times T} \int_{-L/2}^{L/2} D_z d_z \quad (2.9)$$

Considering the above definition of CTDI, the equation for an L-length ion chamber changes to equation 2.9.

$$CTDI_L = \frac{\text{value read from ion chamber } (R) \times f\left(\frac{rad}{R}\right) \times C \times L(mm)}{N \times T} \quad (2.10)$$

f: Irradiation factor from irradiation

C: Ion chamber calibration factor

The CTDI calculation, which refers to the $CTDI_{100}$, for the measurement using a 100 mm long ion chamber, takes the form below.

$$CTDI_{100} = \frac{\text{value read from ion chamber } (R) \times f\left(\frac{rad}{R}\right) \times C \times 100(mm)}{N \times T} \quad (2.11)$$

2.5.1.1. Weighted Computerized Tomography Dose Index ($CTDI_w$)

As the dose distribution in the body changes with depth, the contributions from the body center and its edges to the absorbed dose are taken into consideration separately. For this purpose, the CTDI measurement in the phantom is measured at 5 different points at the center and 4 points near the phantom surface. The values measured at the edge of the phantom are higher than the value at the center. This difference is more pronounced, especially as the phantom diameter increases. For head phantom (16 cm in diameter), the measured values in the center and edges are almost close, while in the body phantom (32 cm diameter) there is a two-fold difference between the center and the edges. In addition, the measured value at 6 o'clock (measurement position under the patient bed) is the lowest due to the bearing reduction (17).

$$CTDI_w = \frac{1}{3}CTDI_{center} + \frac{2}{3}CTDI_{edge} \quad (2.12)$$

$CTDI_{center}$: central measured value

$CTDI_{edge}$: average measurement value of edges.

1/3 and 2/3 are the contributing factors from the center and edges with the order of the absorbed dose.

2.5.1.2. Volumetric Computed Tomography Dose Index ($CTDI_{vol}$)

$CTDI_{vol}$ this is the quantity of dose that takes the pitch factor into account in helical scans. When the Pitch factor is greater than 1, the gaps between the cross-sections will increase compared to the axial scan, and when they are smaller than 1, they will decrease and the sections will overlap. Therefore, CTDI will change depending on the pitch factor. The quantity that takes account the Pitch factor is calculated as follows.

$$CTDI_{vol} = CTDI_w \times \frac{N \times T}{I} \quad (2.13)$$

I : 1-turn rotation of the beam tube is the table travel distance.

$$\frac{1}{p} = \frac{N \times T}{I} \quad (2.14)$$

$$CTDI_{vol} = \frac{CTDI_w}{p} \quad (2.15)$$

2.5.1.3.Dose Length Product (DLP)

The radiation dose and risk in CT are related to the type and amount of irradiated anatomical structure. The CTDI is an indication of the single-dose mean dose in the central region of the scanned volume along an adjacent series scan. However, we need to know the total radiation dose accumulated in the patient for the risk of ionizing radiation. DLP was defined for the total dose accumulated in CT. Calculated as follows and the unit is mGy-cm.

$$DLP = CTDI_{vol} \times L \quad (2.16)$$

L: Total length scanned along the z-axis in a single-array irradiation

2.6.Image Quality Parameters in Computed Tomography

2.6.1.Noise on Computed Tomography

Contrast resolution corresponds to the ability to recognize subtle changes in gray tones and remove them from image noise. Signal-to-noise ratio (SNR) in the image is used to determine the contrast resolution. The contrast resolution relates to structures that produce small changes in signal intensity, which makes it difficult to detect the structure from a noisy background. Low precision measurements have a higher noise level. On medical images, sensitivity should be related to the amount of noise (3).

The contrast ratio (CNR) of the noise is a measure of the signal level independent of the object size in the presence of noise. As shown in figure 2.30, the contrast is calculated from the background (x_{BG}) ROI and the difference between the average grayscale(x_s) of a region of interest plane and an ROI in the background.

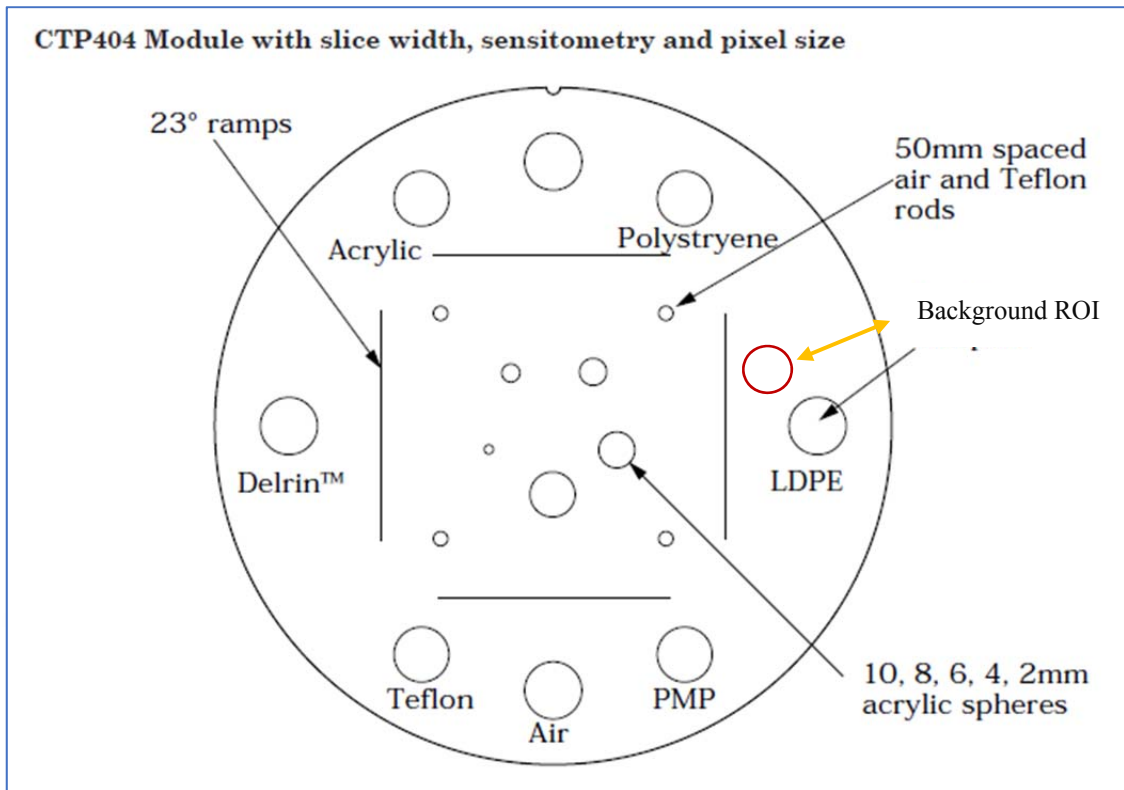


Figure 2.30. CT images of Catphan 600 (CTP404) modules for measuring CNR.

Thus, the CNR is given by

$$CNR = \frac{X_s - X_{bg}}{\sigma_{bg}} \quad (2.17)$$

The SNR is a CNR-like metric, but the size and shape of the displayed object is included in the calculation. SNR does not require homogeneity of the test object, but the background must be homogeneous (1). SNR is one of the most significant measurements defining the specificity of an object. From a single ROI, the SNR value is calculated. As shown in equation 2.18, SNR equals to mean counts in ROI over standard deviation.

$$SNR = \frac{\text{mean counting in ROI}}{\sigma} \quad (2.18)$$

2.6.2. CT Number Accuracy

The CT number consistency is that the CT numbers of the phantom do not change when the same phantom is displayed at different slice thicknesses at different times. Consistency and homogeneity of the CT number are factors that affect the accuracy of the CT number (3). The accuracy of the CT number for a given phantom is that the position of the selected ROI or the imaginary position of the scanner does not change with respect to the iso-center.

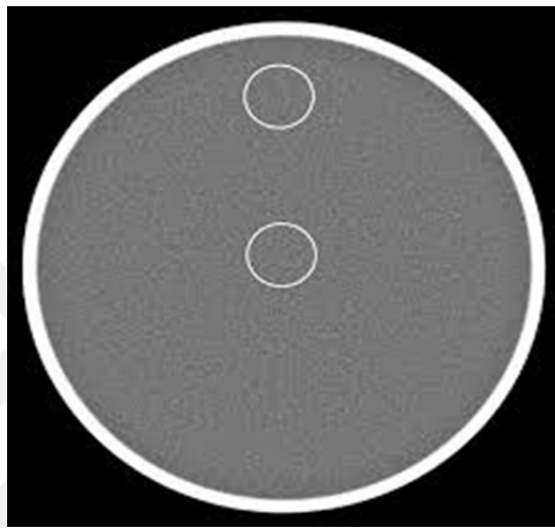


Figure 2.31. Water phantom for CT number uniformity and noise measurement.

2.6.3. Low-Contrast Spatial Resolution

The main task of the diagnostic CT system is the detection of lesions or tissue of interest visually. Therefore, distinguishing tissues or lesions is an important criterion for image quality. The low contrast resolution defines the ability to distinguish between tissues that show little difference in attenuation coefficients after the x-ray passes through the object of interest. In order to determine the low contrast resolution of a system, objects with a very small attenuation coefficient difference from the background are often used. Since the difference between these two structures is minimal, noise in the image becomes an important factor. CNR is calculated using phantom images and is a measure of evaluation of low contrast resolution (18).

2.6.4.High-Contrast Spatial Resolution

The high contrast spatial resolution of a CT means that it can analyze objects placed near the CT well. High contrast resolution can also be measured with phantoms containing bar patterns of various spatial frequencies as indicated by the CATPHAN® phantom. By visually examining the different bar patterns, only the best bar model (and hence the highest spatial frequency) can be determined, which can only be solved or barely separated. It is assumed that the limiting resolution value usually represents 5% of the Modulation Transfer Function (MTF) (19). Although this test is useful, the result is somewhat subjective and represents only one point on the MTF curve. Sub-spatial frequencies provide little information about behavior (20).

As shown in Figure 2.32, pairs of different density lines found in the displayed phantom are used to determine the resolution. Resolution is specified as one pair per centimeter (lp / cm) or per millimeter (pairs / mm) (17). Each bar set represents a specific line pair. It examines the ability of a CT scanner to solve different bar patterns and predicts the spatial resolution capability of the system under the prescribed conditions.

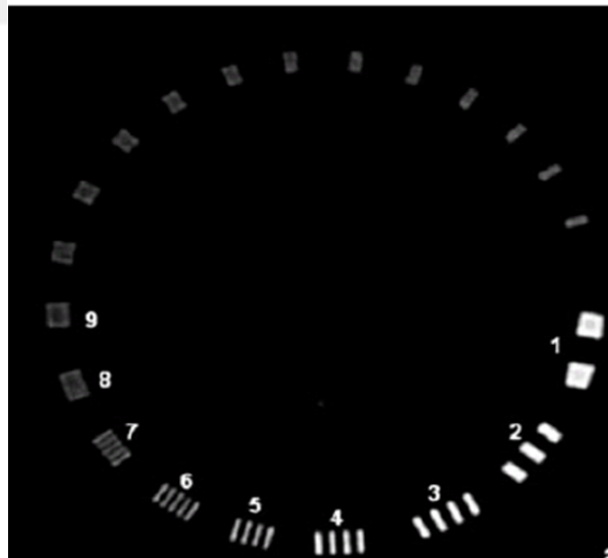


Figure 2.32.A restructured portion of a CATPHAN® phantom

However, the modulation transfer function (MTF) is a more scientific measure of the spatial resolution properties of an imaging system compared to the above-mentioned resolution determination method (3). MTF is defined as the ratio of output modulation to input modulation and measures the response of a system to different frequencies. The MTF of most systems drops rapidly at high frequencies. The input frequency at which the system response approaches zero is called the limiting frequency. MTF is determined by the Fourier transform of the point spread function (PSF) (1). Spatial field propagation functions there are mathematical relationships between PSF, LSF (Line spread function) and ESF (Edge spread function). The LSF is computed by convolving the PSF with a line (21).

Joseph Fourier, a French mathematician of the nineteenth century, developed a method for separating a series of sinusoidal waves. The LSF's Fourier transform (x) calculates the entire MTF curve (3). Almost all periodic functions of medical imaging can be represented by a Fourier Series. The Fourier transform is an algorithm that transforms a signal into a series of sinewaves that, when a spatial or time-domain signal is collected, is copied. Fourier calculations are a routine part of the medical imaging system. For CT reconstruction, Fourier transforms are used to filter through filtered reverse projection. The LSF's Fourier transform (x) calculates the entire MTF curve. Before calculation, LSF (x) is normalized to have a unity field (21).

3.MATERIAL and METHOD

In this study, PET / CT tomography device in Yeditepe University Specialized Hospital was used. In this system, both filtered back projection and iterative Reconstruction algorithm can create tomography. Computed tomography dose index (CTDI) values, CTDI phantom, and 10cm pen-type ion chamber were used for different irradiation parameters. Cathpan 600 phantom was used for image quality evaluation. Image quality parameters were evaluated by using IMAGE J and IQ WORK (free software).

The irradiation parameters of the tomography system were 120 kVp and three different mA values (65,125 and 255). CTDI values for these different mA values will be measured and compared with the values given by the system. Both 2.5 mm and 5 mm tomographic sections were obtained.

Filtered back projection and iterative reconstruction parameters were obtained by using standard and detail filters of Catphan 600 phantom at 20,40,60,80 and 100 values. Image quality parameters such as CNR, SNR, and MTF were evaluated for all Reconstruction methods from Catphan 600 phantom images.

3.1.CTDI Measurements

For this measurement 100 mm ion chamber (820204-C Xi CT detector, designed by Unfors Raysafe made in Sweden), 32 cm whole-body phantom, display (8201023-D Xi base unit w / mas, designed by Unfors Raysafe made in Sweden) and PET / CT Device (GE) was used. The entire body phantom was positioned aligned with the internal laser lights of the CT device.

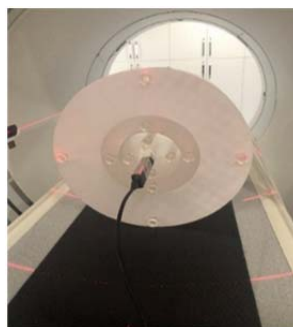


Figure 3.1.Ion chamber on the center of CTDI phantom

As shown in Figure 3.1, the ion chamber was placed in the center of the phantom and 65,125 mA and 255 mA axial scanning were performed under the specified measurement conditions (measurement conditions: 120 kVp, 5 mm, 1sec single section axial scan).

As shown in Figure 3.2, the ion chamber was then moved to the locations around the entire body phantom as shown in figure 3.2 (north, east, south and west) respectively, and axial scanning was performed under the same scanning conditions. The ion chamber readings were then recorded to compare with the results of the system.

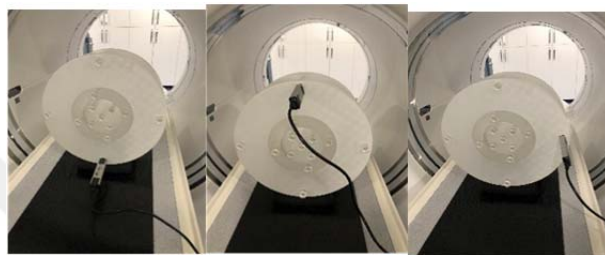


Figure 3.2. Ion chamber positions on phantom

3.2. Measurements for Image Quality Parameters

As shown in Figure 3.3, ‘The image quality phantom Catphan600’ phantom was used in these measurements. The phantom was placed in the patient bed by aligning the internal laser lights as shown in figure 3.4.



Figure 3.3. CT quality assurance phantom, Catphan 600, positioning to test

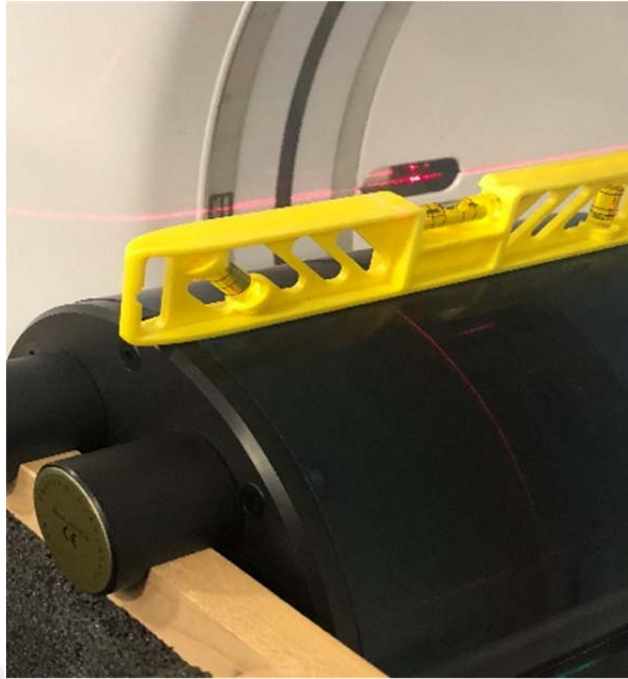


Figure 3.4. Aligning Cathpan phantom with internal laser lights

Before irradiation, the X-Ray tube was warmed and scouted. According to the scout appearance, the FOV was adjusted to 25 cm. Helical scanning of 2.5 mm and 5 mm cross-sectional thickness was performed under defined shooting conditions with a 5 cm gap from the beginning and end of the phantom. Shooting conditions; 120 kVp, rotation time 1s, coverage 40 mm, pitch 0.984 and 65,125,255 mA respectively.

FBP was applied to 65 mA standard phantom image and the resulting image was recorded for calculations. Then, 20,40,60,80 and 100 ASIR were applied to 65 mA standard images, respectively. The same procedures were repeated for 125 mA and 255 mA.

65 mA Detail phantom image FBP was applied and the image was saved for calculations. Then, 20,40,60,80 and 100 ASIR were applied to 65 mA detail phantom images, respectively.

3.2.1. MTF Measurements

MTF measurements were made from the Cathpan 600 (CTP 591 bead geometry module) phantom as shown in figure 3.5, images obtained as a result of these applications.

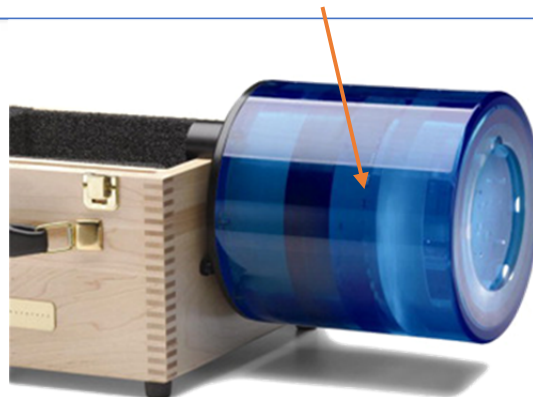
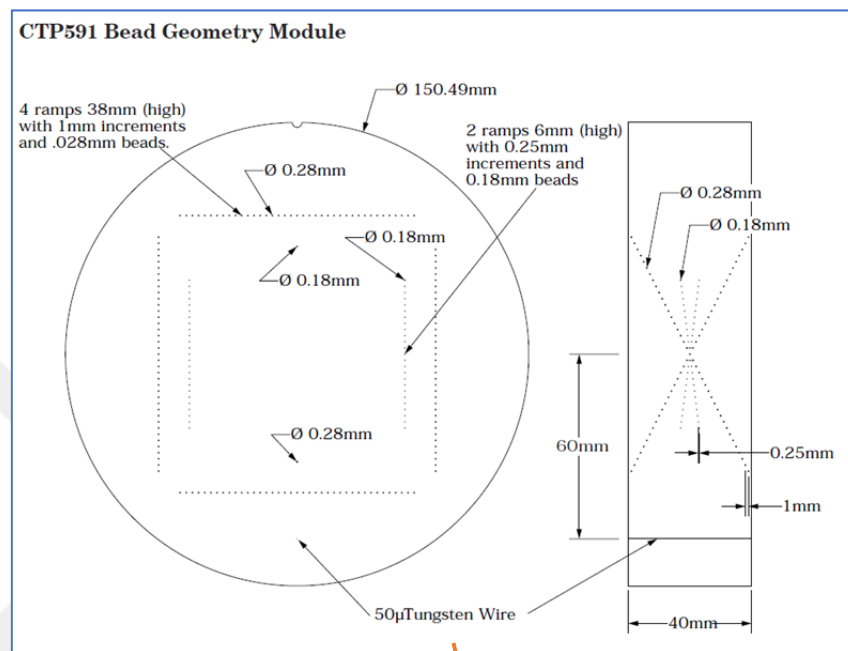


Figure 3.5. Cathpan 600 phantom (CTP 591 module)

Images were transferred from RadiAnt Dicom Viewer and MTF2, MTF10 and MTF50, and calculations were made using the IQ work program as shown in figure 3.6. This calculation was repeated for all images taken.

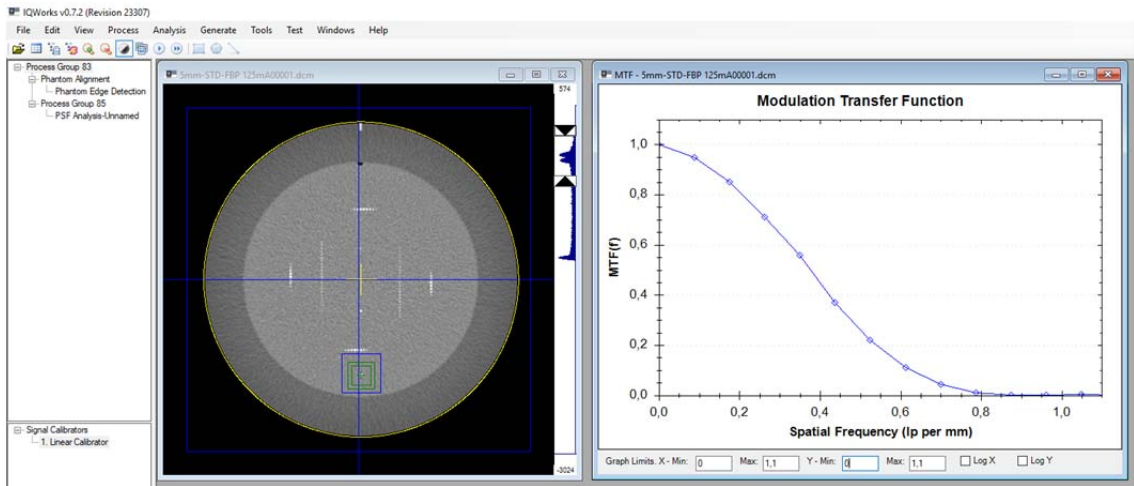


Figure 3.6. IQ works program for MTF calculation

3.2.2. CNR Measurements

Images were transferred from RadiAnt Dicom Viewer and calculations were made using the ImageJ program as shown in figure 3.7. The contrast is calculated from the background ROI and the difference between the average grayscale of a region of interest plane and an ROI in the background.

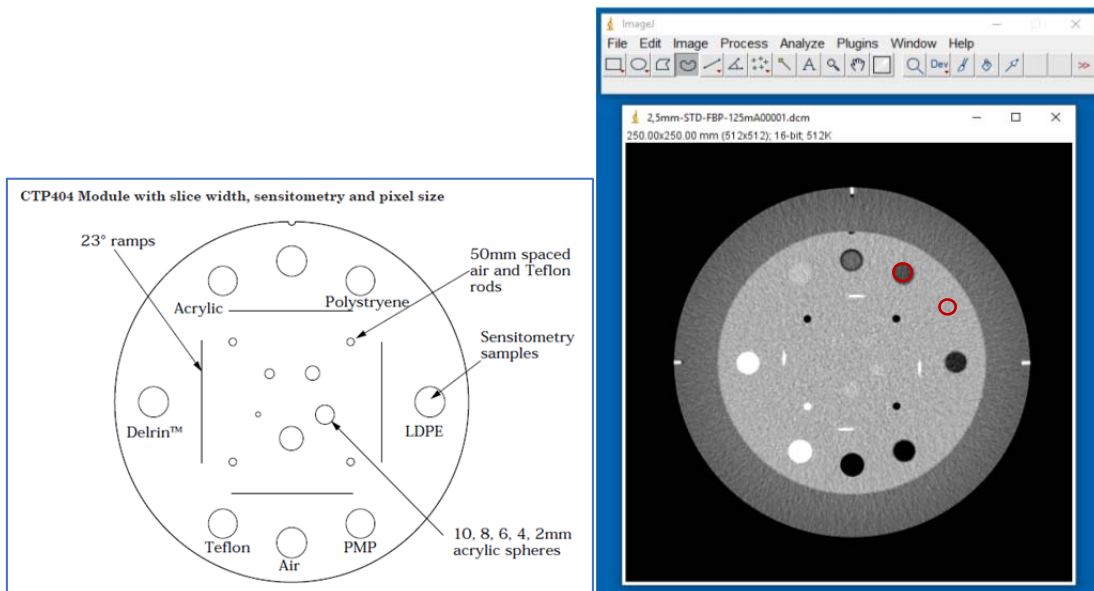


Figure 3.7. CTP 404 Module of. Cathpan 600 phantom ImageJ program for CNR measurement

CNR values of sensometric objects as shown in figure 3.7 with different densities in the phantom were calculated and recorded with ImageJ program for images taken at different slice thicknesses (2.5 and 5 mm) and different mA (65,125 and 255) values.

3.2.3. SNR Measurements

Images were transferred from RadiAnt Dicom Viewer and calculations were made using the ImageJ program. The values of the largest size supra in the low contrast modulus of the Cathpan phantom as shown in figure 3.8 were used for SNR calculations.

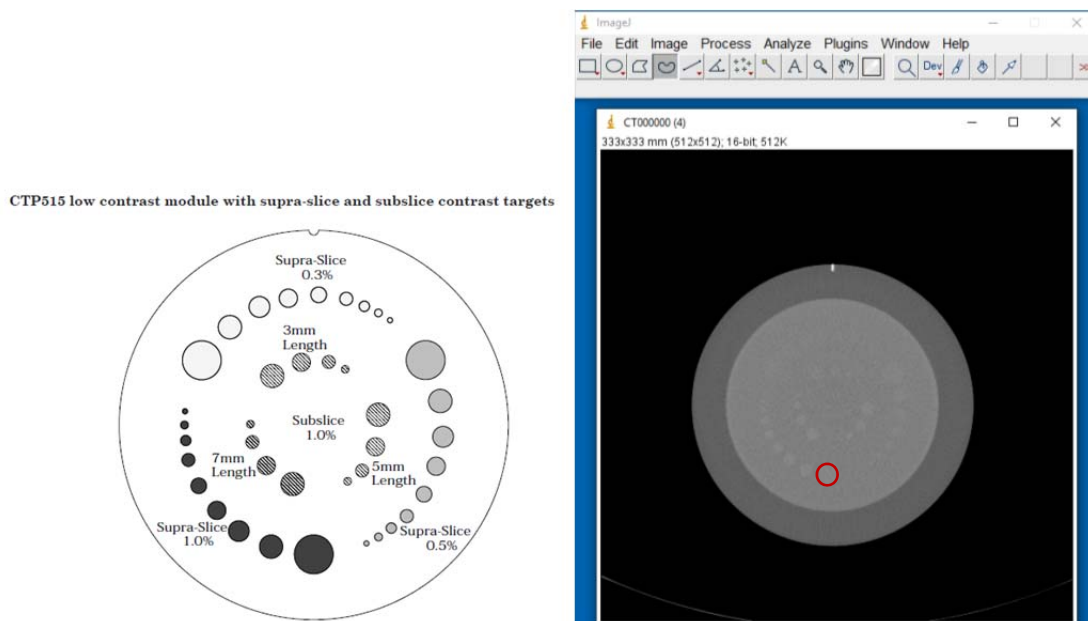


Figure 3.8. CTP 515 Low contrast module of Cathpan 600 phantom

4.RESULTS and DISCUSSION

4.1. CTDI Measurements

65,125 and 255 mA, 120 kVp, 5 mm single section axial scanning, rotation time of 1 second, the system shows the CTDI values as follows.

Table 4.1.CTDI Result of 65 mA

The position of the ion chamber on the phantom	1st shot ion chamber reads (μGy)	2 nd shot ion chamber reads (μGy)	Average (μGy)
Center	245.6	243.7	244.6
North	510.7	520.5	515.6
East	498.9	513.1	506.0
South	413.5	415.0	414.2
West	510.4	510.1	510.2

CTDI (system) = 8.01 mGy

The deviation of the dose measured according to the criteria announced in EC No 162 from the specified dose should be less than 20%.

Table 4.2. CTDI Result of 125 mA

The position of the ion chamber on the phantom	1st shot ion chamber reads (μGy)	2 nd shot ion chamber reads (μGy)	Average (μGy)
Center	482.1	482.5	482.3
North	1112	1109	1111
East	878.9	880.2	881
South	850.9	852.1	852
West	1090	1086	1088

CTDI (system) = 15.3 mGy

Table 4.3.CTDI Results of 255 mA

The position of the ion chamber on the phantom	1st shot ion chamber reads (μGy)	2 nd shot ion chamber reads (μGy)	Average (μGy)
Center	916.3	922.2	919.2
North	1948	1983	1965
East	1195	1184	1189
South	1575	1566	1570
West	1907	1936	1921

CTDI (system) = 31.01 mGy

Table 4.4. Summary of CTDI measurements

mA	$CTDI_{system}$	$CTDI_{measurement}$	Difference (%)
65	8.01mGy	8.11mGy	~%1.5
125	15.3mGy	16.22mGy	~%6
255	31.01mGy	28.27mGy	~%9

CTDI value calculated according to equations 2.11 and 2.12. CTDI results are in the range of acceptance values specified above. As can be seen in Table 4.4, the differences between CTDI and the values given by the system were found to be below ten percent. According to this result, the CTDI accuracy of the system has been proved.

4.2.MTF Measurements

MTF results for standard filter and 125 mA are given in figure 4.1. Only the 125 mA and 5 mm slice thickness results are given for clarity. The other figures for 65 and 255 mA and 2.5 mm slice thickness are given in Appendix I.

It is found that the MTF increases with the use of iterative reconstruction. The increment is higher for mid-frequencies than low and high frequencies.

This pattern can also be seen in figure 4.2. Frequency increment at 10th and 50th percent of MTF is increasing with iterative reconstruction use, while there is no similar pattern is seen in 2th percent of MTF.

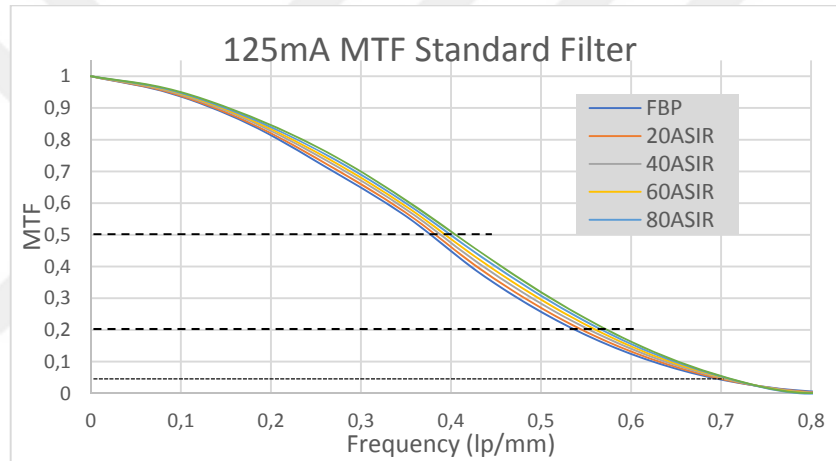


Figure 4.1. MTF results for standard filter and 125 mA

Fifty percent of MTF has been observed to improve with the use of the ASIR algorithm. A small improvement was observed when the value of ten percent of MTF. MTF 2%, which is considered as the resolution value of the system, did not change as a result of the use of the ASIR algorithm.

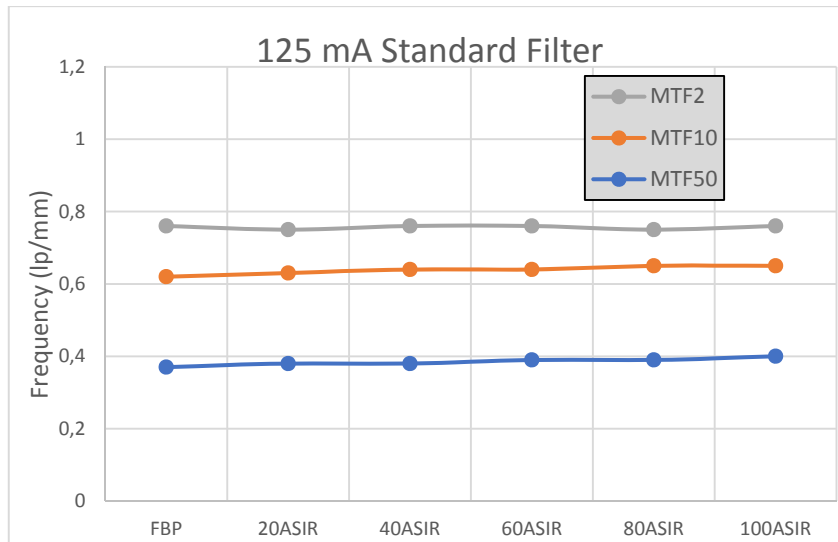


Figure 4.2. Percentage values of MTF with Standard Filtr

A similar result as in Figure 4.1 was observed in figure 4.2. Fifty percent and ten percent improvement in the value of MTF, while two percent difference was not observed.

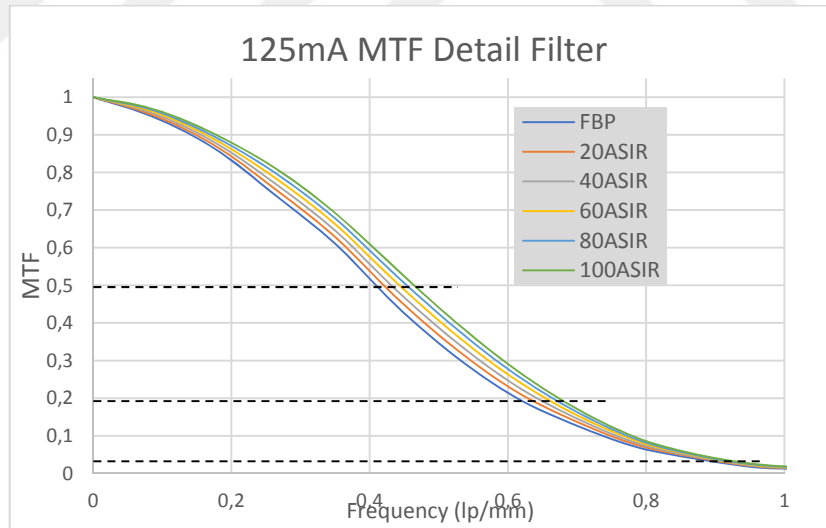


Figure 4.3. MTF results for Detail filter and 125 mA

Similar results were observed for MTF results in standard filters. However, improvement in detail filter with ASIR algorithm was more.

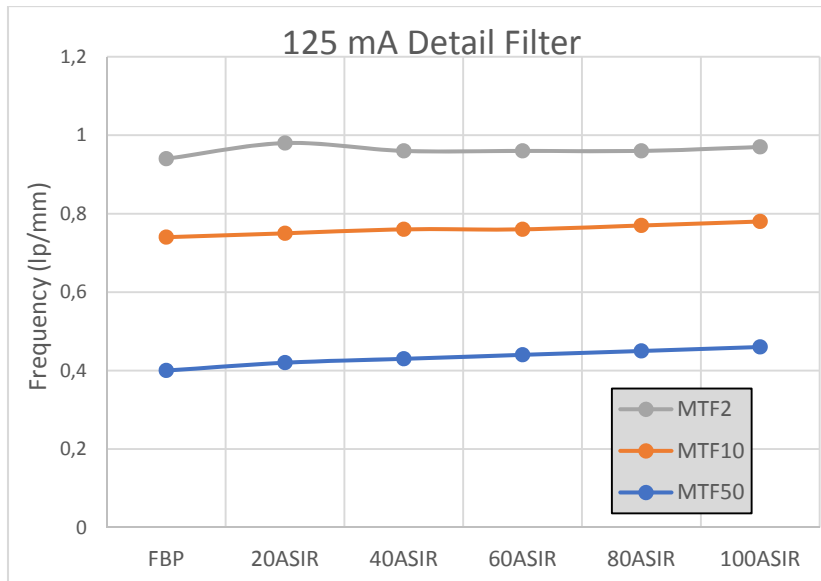


Figure 4.4. Percentage values of MTF with Detail Filter

A similar pattern was also observed in detail filter MTF measurements. Due to the use of sharper filter MTF values are higher as expected. (Figure 4.4 can be compared with figure 4.2.)

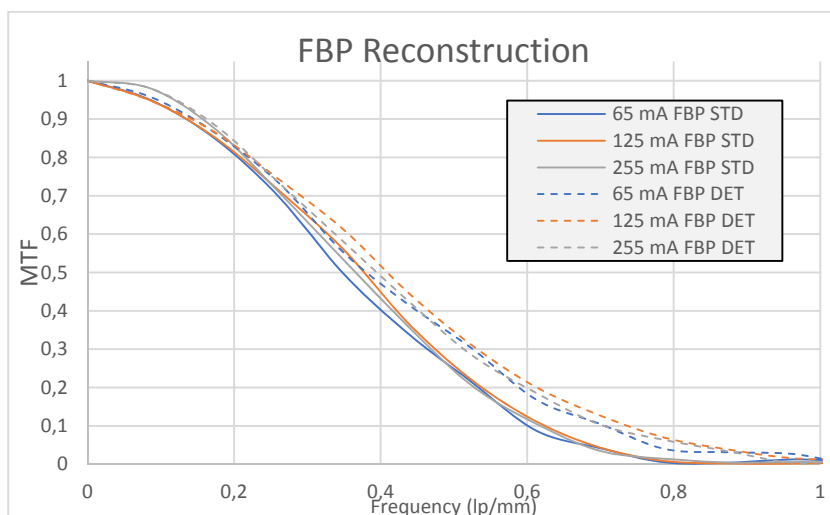


Figure 4.5. MTF graphs for different mA values and reconstruction filters.

There was no major difference in MTF values with mA change. Here, MTF values are normally not expected to change, but because the noise in the image changes, differences in measurement results have occurred.

The MTF values in the detail filter were better than expected when compared to the standard filter. Because the detail filter passes higher frequencies better.

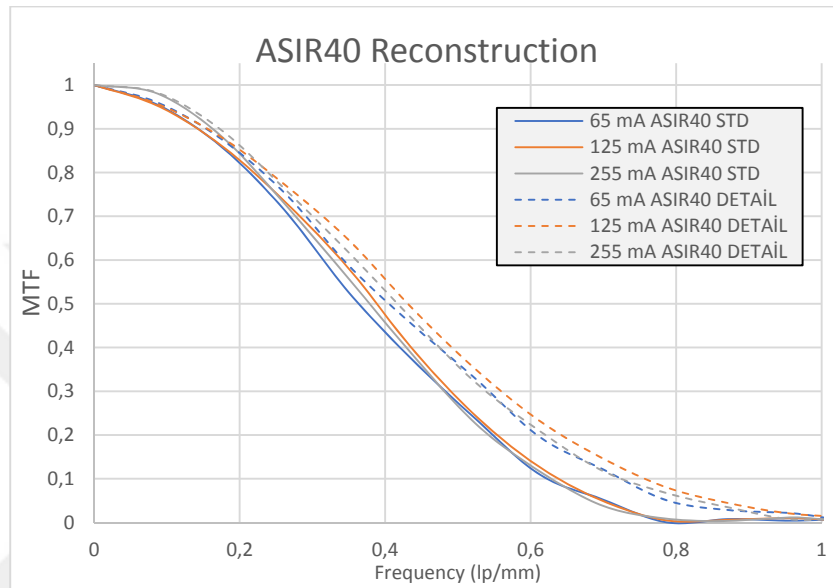


Figure 4.6. MTF graphs for different mA values and ASIR40 reconstruction filters.

The reason for choosing the ASIR40 algorithm as the evaluation criterion in this study is that manufacturers use ASIR percentage between 30 and 50 to contribute to the patient dose.

It was also observed that ASIR algorithms used here contributed to the increase of MTF compared with the result.

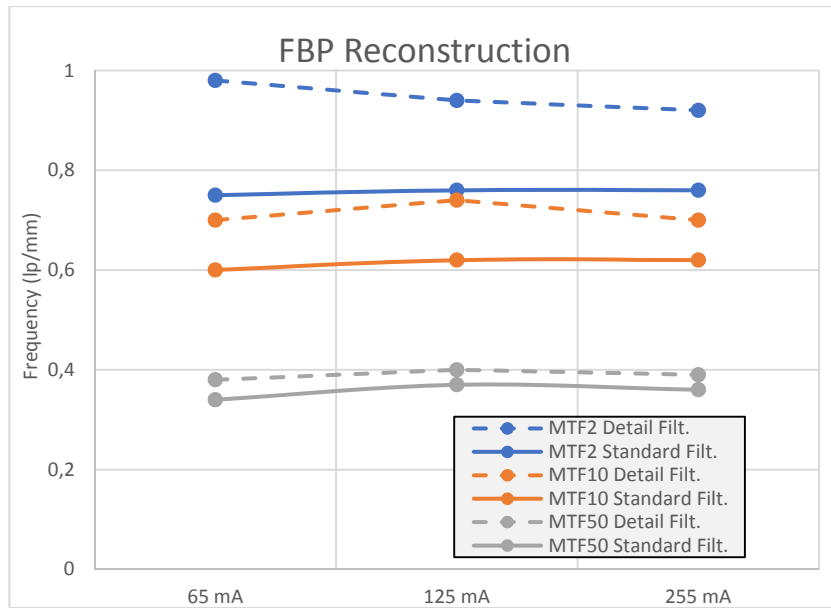


Figure 4.7. MTF percentage values graphs for different mA and reconstruction filters

Tube flow is not expected to have an effect on MTF. As seen in Figure 4.7, the MTF2 detail filter is thought to be high because of the noise in the image used in the calculation of MTF.

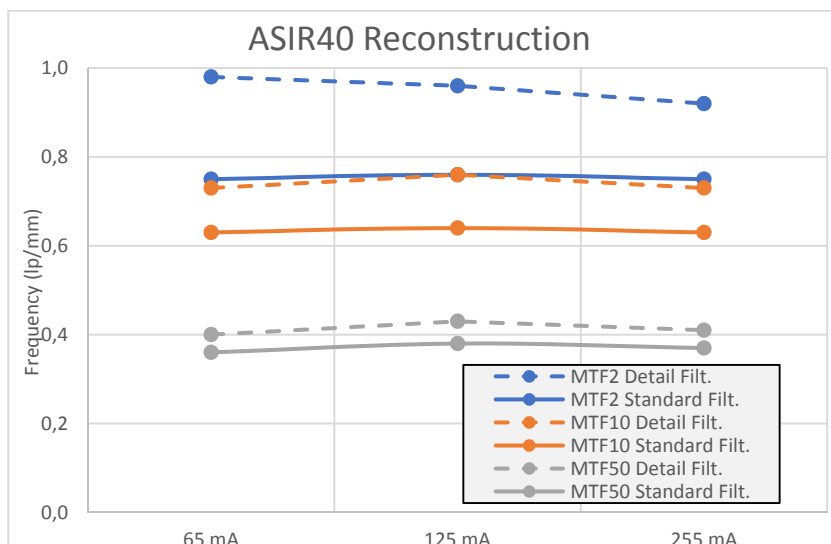


Figure 4.8. MTF percentage values graphs for different mA and ASIR40 reconstruction filters

Tube flow is not expected to have an effect on MTF. As seen in Figure 4.8, MTF2 detail filter is thought to be high because of the noise in the image used in the calculation of MTF.

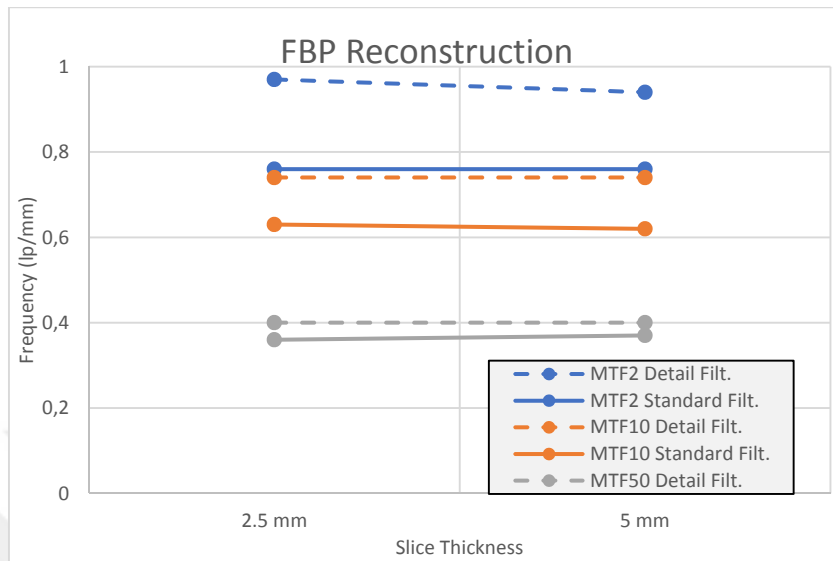


Figure 4.9. MTF percentage values graphs for different slice thickness and reconstruction filters

As seen in figure 4.9, no change was observed. Slice thickness is not expected to have an impact on resolution.

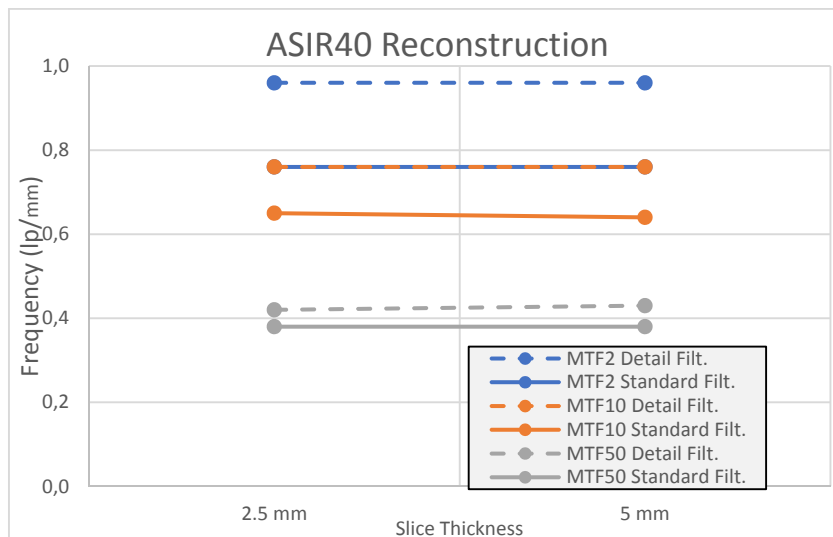


Figure 4.10. MTF percentage values graphs for different slice thickness and ASIR40 reconstruction filters

As seen in Figure 4.10, no change was observed. Section thickness is not expected to have an impact on resolution.

4.3. CNR Measurements

CNR results for standard filter and 125 mA are given in figure 4.11. Only the 125 mA and 5 mm slice thickness results are given for clarity. The other figures for 65 and 255 mA and 2.5 mm slice thickness are given in Appendix I.

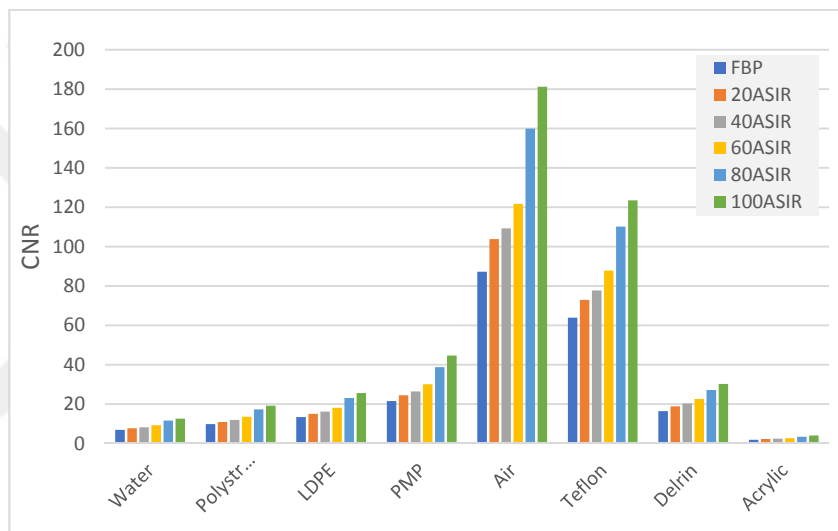


Figure 4.11. CNR results for standard filter and 125 mA

It was observed that the CNR values improved by using the ASIR algorithm in all the materials measured. But this improvement has been more pronounced in the standard filter than the detail filter.

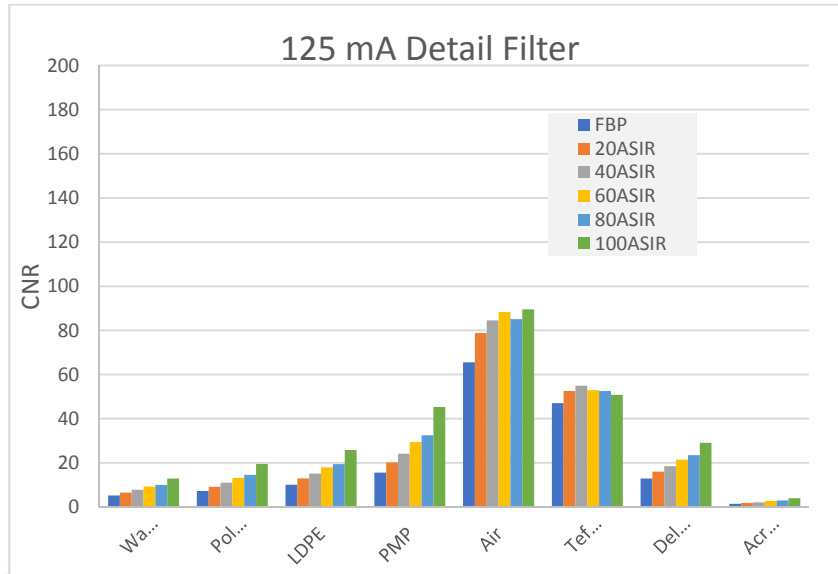


Figure 4.12. CNR results for Detail filter and 125 mA

CNR results for detail filter and 125 mA are given in figure 4.12. Only the 125 mA and 5 mm slice thickness results are given for clarity. The other figures for 65 and 255 mA and 2.5 mm slice thickness are given in Appendix I.

Noise is the reason why the improvement in CNR in the detail filter is less observed than in the standard filter. Since the ASIR algorithm improves this noise, the CNR is improved.

As seen in figure 4.13, three items were selected for comparison in the CNR result. These are water, PMP, and Teflon. Water was chosen because it represents soft tissue, PMP is an occasional value, and Teflon represents bone tissue.

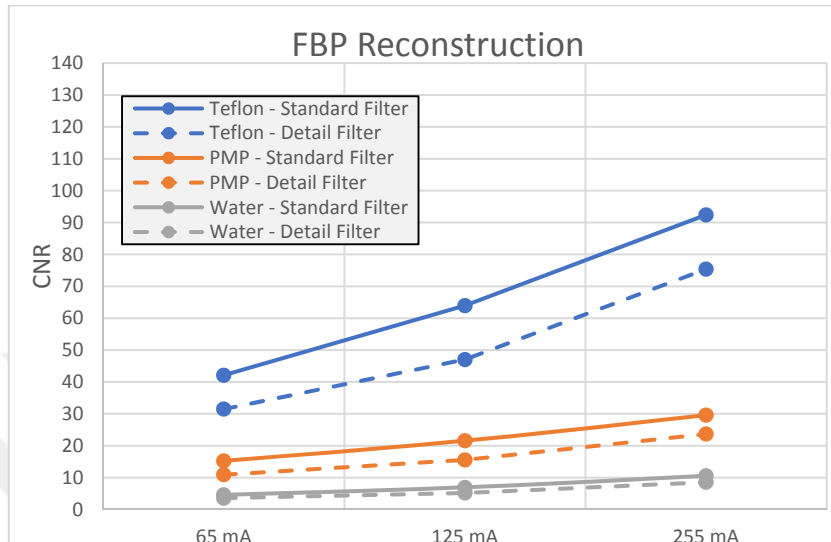


Figure 4.13. CNR graphs for different mA and reconstruction filters

When ASIR and FBP are compared, CNR value is observed higher using ASIR40 Reconstruction than using FBP (figure 4.13 and 4.14).

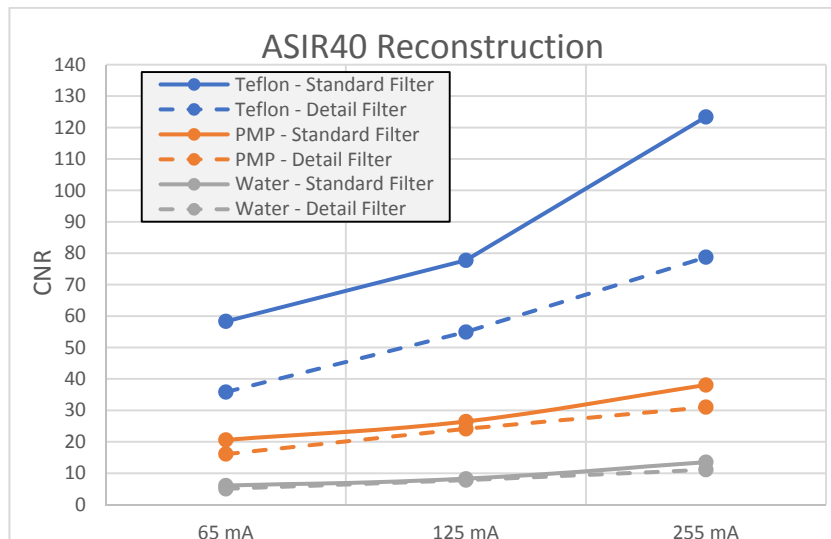


Figure 4.14. CNR graphs for different mA and ASIR40 reconstruction filters

As seen in figure 4.14, the reason for the lower CNR values observed in the detail filter increases the high-frequency noise with the sharp filter and high-frequency detail filter. Due to the effect of this, it was observed that the CNR ratios of the detail filters were lower. But when iterative reconstruction and FBP are compared, CNR loss in the detail filter is less than FBP.

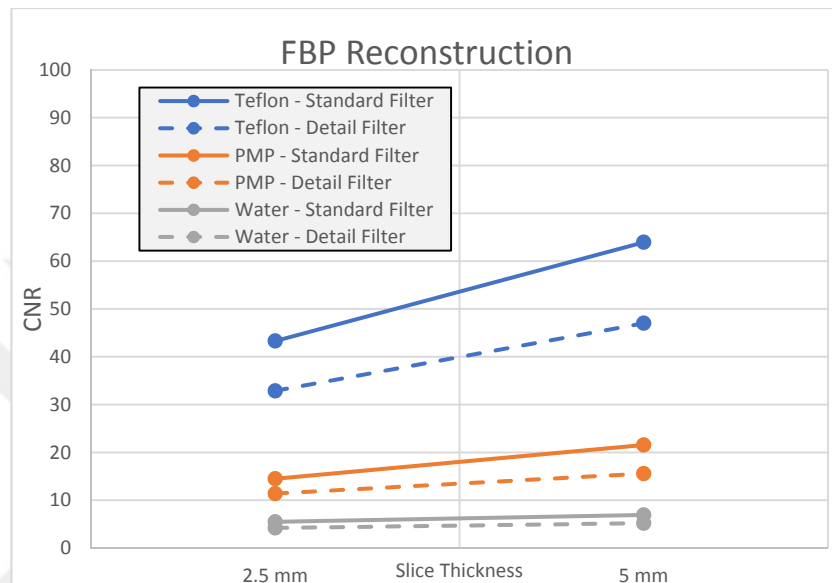


Figure 4.15. CNR graphs for different slice thickness and reconstruction filters

As can be seen from graph 4.15 given above the noise to decrease with increasing section thickness, CNR improved as expected.

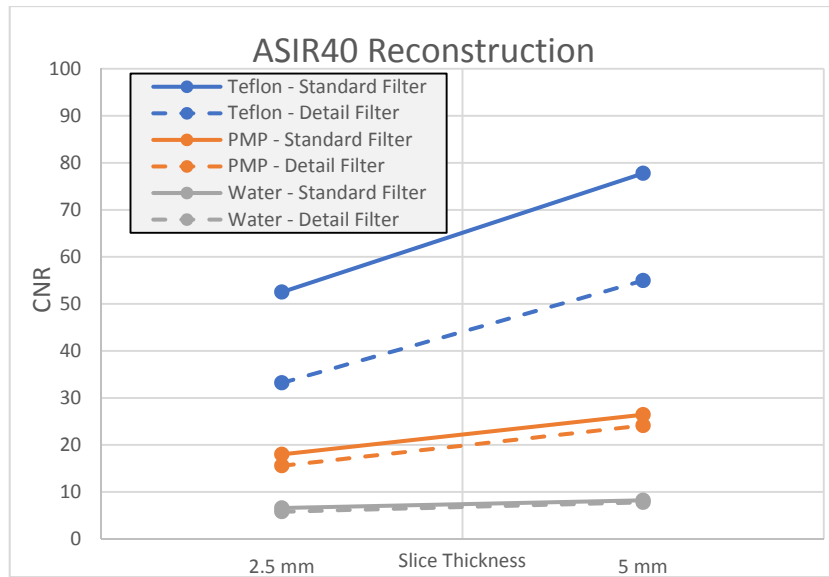


Figure 4.16. CNR graphs for different slice thickness and ASIR40 reconstruction filters

As the thickness of the section increases, CNR rises, but ASIR contributes more to this improvement.

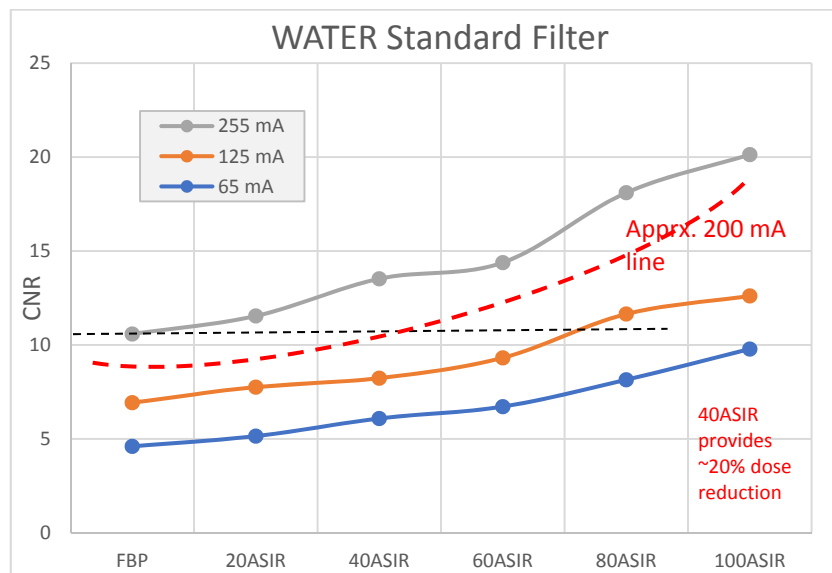


Figure 4.17. CNR results for Water in different mA

Figure 4.17. As shown, the same result was obtained by using 125 mA and ASIR80 instead of the CNR value obtained by FBP 255 mA. If we consider an imaginary two hundred mA line with for forty percent ASIR reconstruction technique proved approximately twenty percent dose reduction.

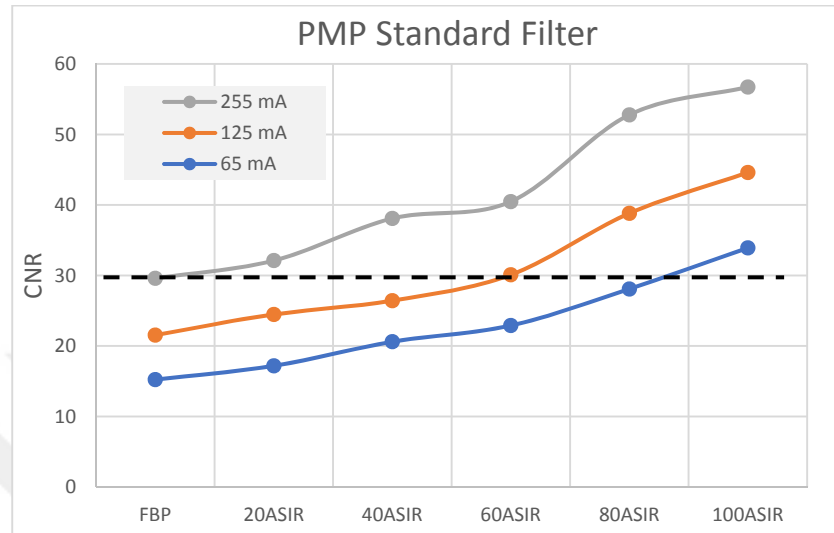


Figure 4.18. CNR results for PMP in different mA

As shown in figure 4.18, the same result was obtained by using 125 mA and ASIR60 instead of the CNR value obtained by FBP 255 mA. It is seen that the CNR value obtained at 255 mA with FBP can be obtained by using the ASIR 80 algorithm with 65 mA value.

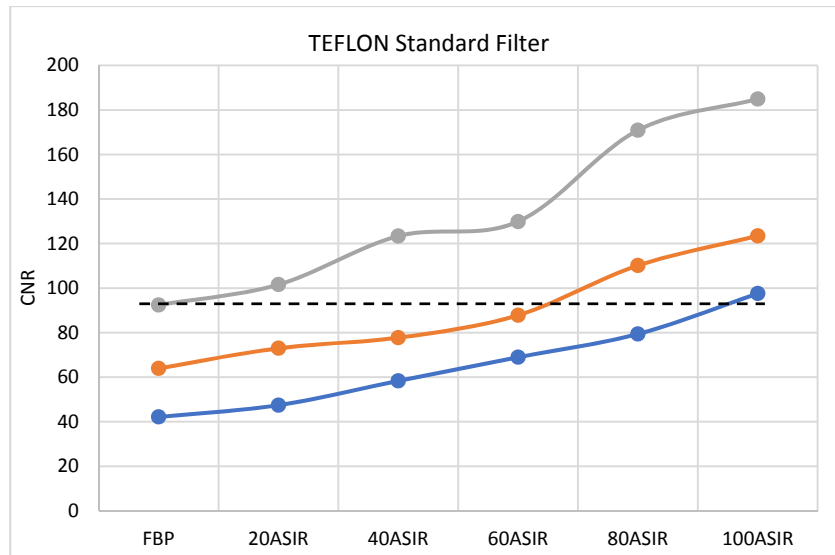


Figure 4.19. CNR results for Teflon in different mA

As shown in figure 4.19, the same result was obtained by using 65 mA and ASIR100 instead of the CNR value obtained by FBP 255 mA. And the result is almost 255 mA and 125 mA using the ASIR60.

4.4. SNR Measurements

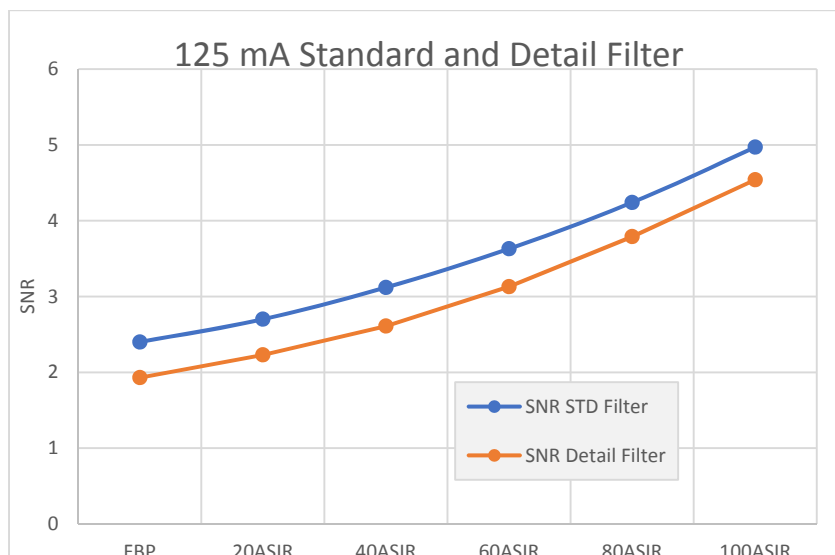


Figure 4.20. SNR result for Standard Filter and Detail Filter with FBP.

Figure 4.20. As seen in the measurements made according to the homogeneous part of the phantom, the SNR rate increases as the percentage of ASIR increases.

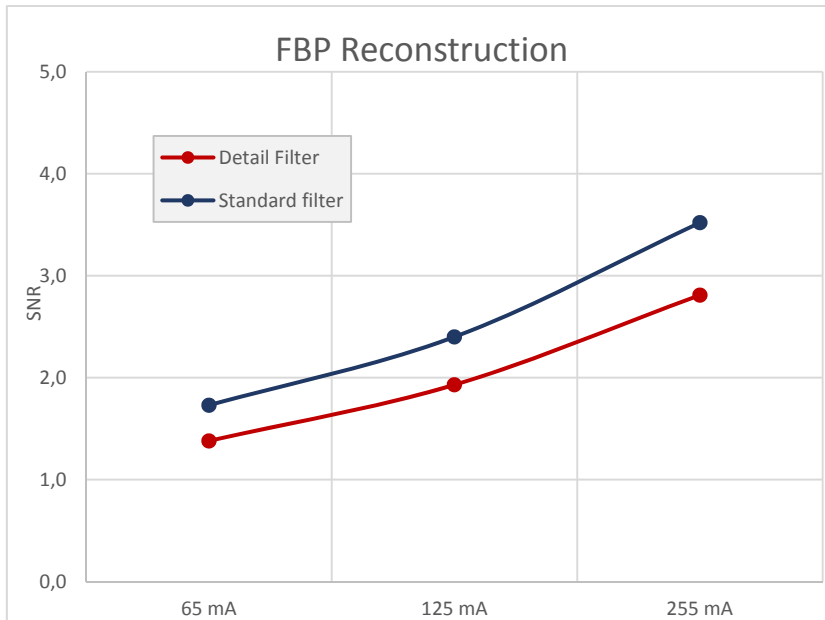


Figure 4.21. SNR results in different mAs and FBP.

As a result of the increase in mAs the SNR value is increased for standard and detail filter as shown in figure 4.21. It was observed that SNR value obtained with 125 mAs detail filter was reached by using standard filter at 65 mAs.

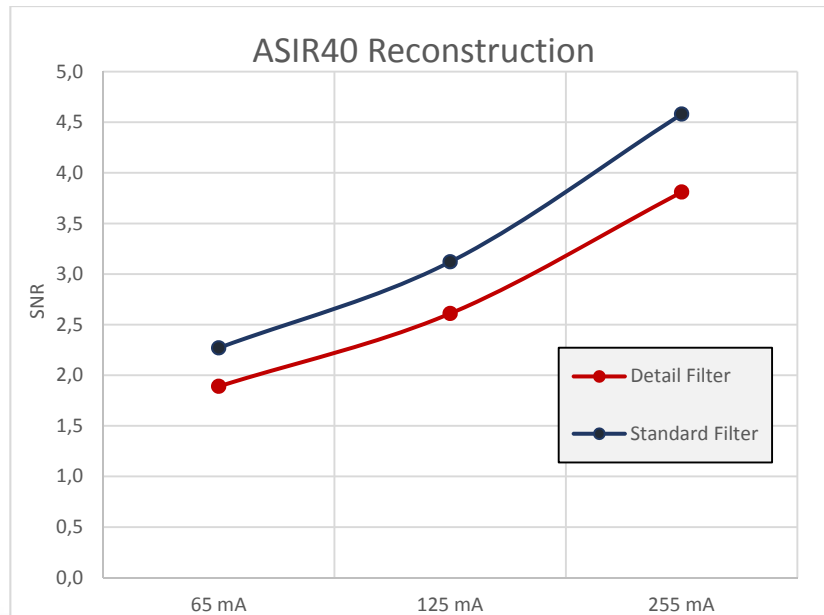


Figure 4.22. SNR result for different mA and ASIR40 Reconstruction filter

Figure 4.22 shows that the use of ASIR increased the SNR value compared to figure 4.21 for both filters. As seen in figure 4.21, the standard filter with 125 mA SNR value is approximately two and a half, figure 4.22 in the same conditions with the use of ASIR, SNR value rises to approximately three and a half value. Likewise, when we look at the results of the detail filter, the use of the ASIR algorithm instead of FBP increased the SNR value which is approximately two values in figure 4.21 to approximately three in figure 4.22.

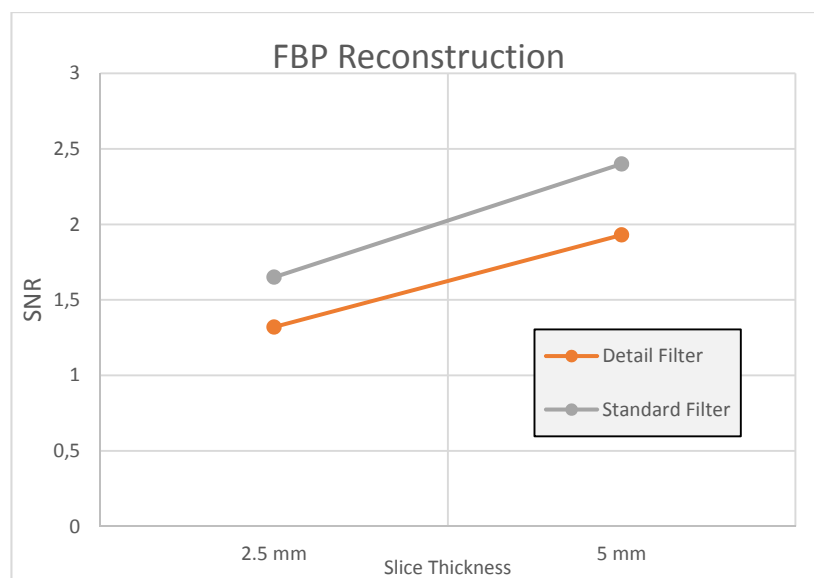


Figure 4.23. SNR graphs for different slice thickness and reconstruction filters

As seen in Figure 4.23, the SNR value increased with increasing slice thickness as expected.

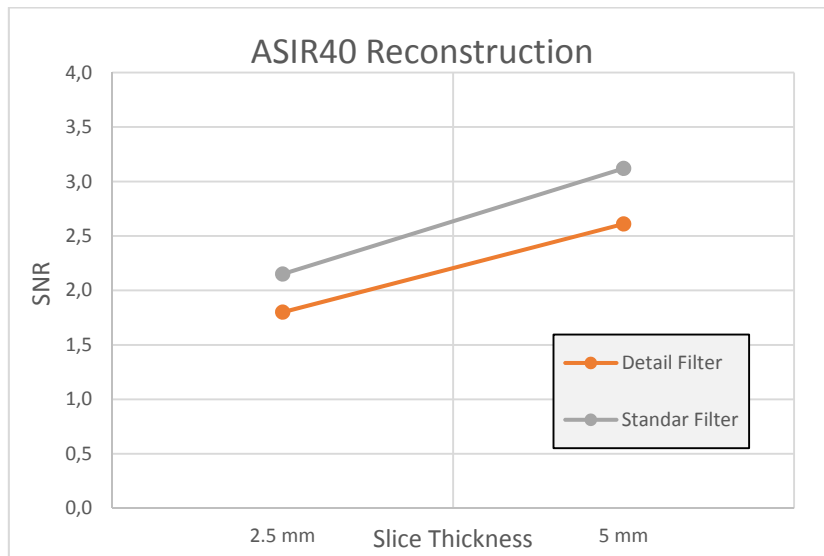


Figure 4.24. SNR graphs for different slice thickness and ASIR40 reconstruction filters

As shown in Figures 4.24 and 4.23, the use of ASIR instead of FBP increased the SNR value. 5 mm slice thickness of the standard filter with the FBP algorithm is seen to be approximately two SNR values and the standard filter using the ASIR algorithm seen in Figure 4.23 is seen that the value of the SNR exceeds two and a half. When the detail filter is examined by the same method, the SNR value increases by approximately half a value.

As a result, it was determined that the image quality parameters were improved with ASIR algorithm. According to these results, with the IR algorithm, the image quality can be maintained and lower quality values (and therefore lower dose values) can be obtained.

5. CONCLUSIONS

In this study, when MTF parameter results are examined, It is found that the MTF increases with the use of iterative reconstruction. The increment is higher for mid-frequencies than low and high frequencies. Frequency increment at 10th and 50th percent of MTF is increasing with iterative reconstruction use, while there is no similar pattern is seen in 2th percent of MTF.

When CNR parameter results are examined, CNR values improved by using the ASIR algorithm in all the materials measured. But this improvement has been more pronounced in the standard filter than the detail filter. Noise is the reason why the improvement in CNR in the detail filter is less observed than in the standard filter. Since the ASIR algorithm improves this noise, the CNR is improved. three items were selected for comparison in the CNR result. These are water, PMP, and Teflon. Water was chosen because it represents soft tissue, PMP is an occasional value, and Teflon represents bone tissue. As a result of the CNR results of water material, ASIR40 algorithm provides a 20 percent dose reduction at 200 mA. The reason for choosing the ASIR40 algorithm as the evaluation criterion in this study is that manufacturers use ASIR percentage between 30 and 50 to contribute to the patient dose. When we look at the SNR parameter, the SNR rate increases as the percentage of ASIR increases.

In CT component of PET / CT device in Yeditepe University Specialized Hospital Nuclear Medicine, quantitative image quality parameters were evaluated at different dose levels and tomography was obtained at lower irradiation conditions at the same image quality. When all the results are examined, in this thesis, the same image quality is obtained with the same image quality as the computed tomography using ASIR algorithm by applying less doses instead of FBP.

6.REFERENCES

1. Hsieh, J. *Computed Tomography, Principles, Design, Artifacts and Recent Advances*. Bellingham, Washington, USA: Wiley Inter-Science; 2009.
2. Ohlerth, S., Scharf, G. Computed tomography in small animals – Basic principles and state of the art applications. *Vet. J.*2007;**173**: 254–271.
3. Bushberg, J., Seibert, A., Leidholdt, E., Boone, J. *The Essential Physics of Medical Imaging*. China: SPi Global; 2012.
4. Hathcock, JT., Stickie, RL. *Veterinary clinics of North America: Small Animal Practice*. United States of America: Elsevier; 2006.
5. Kalender, WA. *Computed Tomography: Fundamentals, System Technology, Image Quality, Applications*. Erlangen, Germany: Publics Publishing; 2011.
6. Defrise, M., Townsend, D., Geissbuhler, A. Implementation of three-dimensional image reconstruction for multi-ring positron tomography. *Phys Med Biol*. 1990;**35(10)**:1361–1372.
7. Bailey, D.L., Humm, J.L., Todd-Pokropek, A., Van Aswegen, A. *Nuclear Medicine Physics: A Handbook for Teachers and Students*. Vienna: International Atomic Energy Agency; 2014.
8. Funama Y, Taguchi K, Utsunomiya D, Oda S, Yanaga Y, Yamashita Y, Awai K. Combination of a low-tube-voltage technique with hybrid iterative reconstruction (iDose) algorithm at coronary computed tomographic angiography. *J Comput Assist Tomogr* 2011;**35**:480-485.
9. Sato J, Akahane M, Inano S, Terasaki M, Akai H, Katsura M, Matsuda I, Kunimatsu A, Ohtomo K. Effect of radiation dose and adaptive statistical iterative reconstruction on image quality of pulmonary computed tomography. *Jpn J Radiol* 2011;**30**:146-153.
10. WilleminckM.J. *Iterative Reconstruction for Cardiopulmonary Computed Tomography*. The Netherlands, Utrecht University, 2015.
11. Kerl JM, Bauer RW, Maurer TB, Aschenbach R, Korkusuz H, Lehnert T, Deseive S, Ackermann H, Vogl TJ. Dose levels at coronary CT angiography--a comparison of Dual Energy-, Dual Source- and 16-slice CT. *Eur Radiol* 2011;**21**:530-537.
12. Andersena, H.Völgyesb D.Catrine A. and Martinsen T.; 2018; **5**: 35-40.

13. Prakash P, Kalra MK, Digumarthy SR, Hsieh J, Pien H, Singh S, Gilman MD, Shepard JA. Radiation dose reduction with chest computed tomography using adaptive statistical iterative reconstruction technique: initial experience. *J Comput Assist Tomogr* 2010;**34**:40-45.
14. Sagara Y, Hara AK, Pavlicek W, Silva AC, Paden RG, Wu Q. Abdominal CT: comparison of low dose CT with adaptive statistical iterative reconstruction and routine-dose CT with filtered back projection in 53 patients. *AJR Am J Roentgenol* 2010;**195**:713-719.
15. GE Healthcare. Computed Tomography: ASiR* High Image Quality and Low Dose: Forget compromise. Available via <http://www.gehealthcare.com/euen/ct/products/Asir/>. Accessed Nov 2012).
16. McCollough, C. Leng, S. Yu, L. Cody, D. Boone, J. and McNitt-Gray, M. CT Dose Index and Patient Dose: They Are Not the Same Thing. *Radiol* 2011;**259**: 311-316.
17. Fleischmann D, Boas FE. Computed tomography--old ideas and new technology. *Eur Radiol* 2011;**21**:510-517.
18. Verdun, F.R., Denys, A., Valley, J.F., Schnyder, P. and Meuli, R.A. Detection of Low Contrast Objects: Experimental Comparison of Single-and Multi-Detector Row CT with a Phantom. *Radiology*2002;**223**: 426-431.
19. McCollough C.H. and Zink F.E., *Performance Evaluation of CT Systems*, in Categorical Courses in Diagnostic Radiology Physics: CT and US CrossSectional Imaging, L. W. Goldman and J. B. Fowlkes, Eds., Elsevier: Oak Brook. 2000. p.189–207.
20. P. M. Joseph and C. D. Stockham, The influence of modulation transfer function shape on computed tomographic image quality. *Radiology* 1982; **145**: 179–185
21. Boone, JM., Determination of the pre-sampled MTF in computed tomography. *Med Phys* 2001;**28**: 356–360.

APPENDIX 1: MEASUREMENT RESULTS for 65 mA and 255 mA

MTF Results for 65 mA and 5 mm Slice Thickness

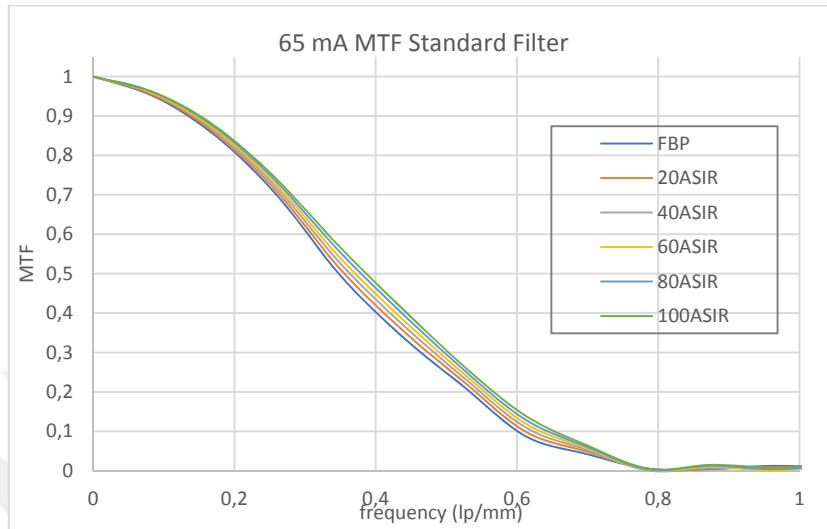


Figure A.1. MTF graphs for standard filter

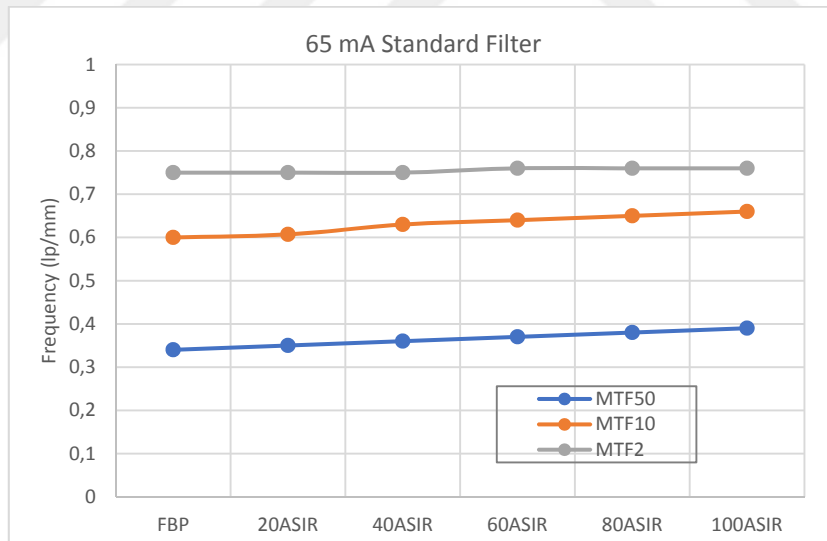


Figure A.2. MTF percentage graphs for standard filter

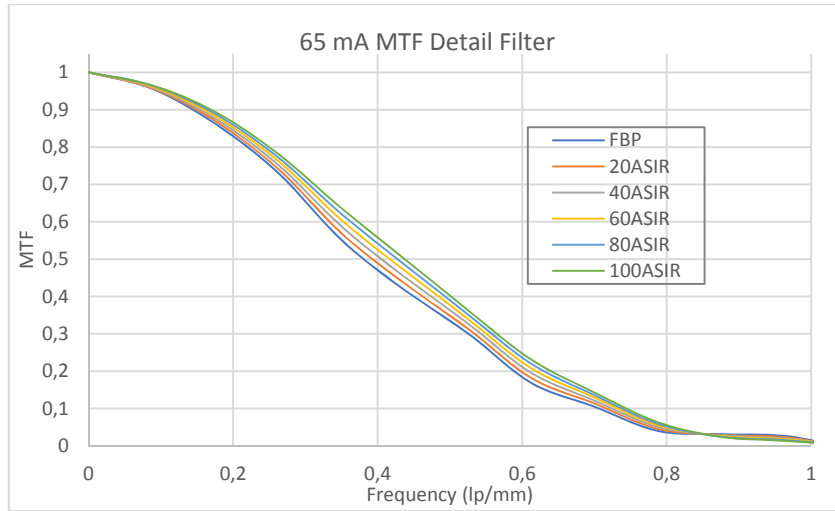


Figure A.3. MTF graphs for detail filter

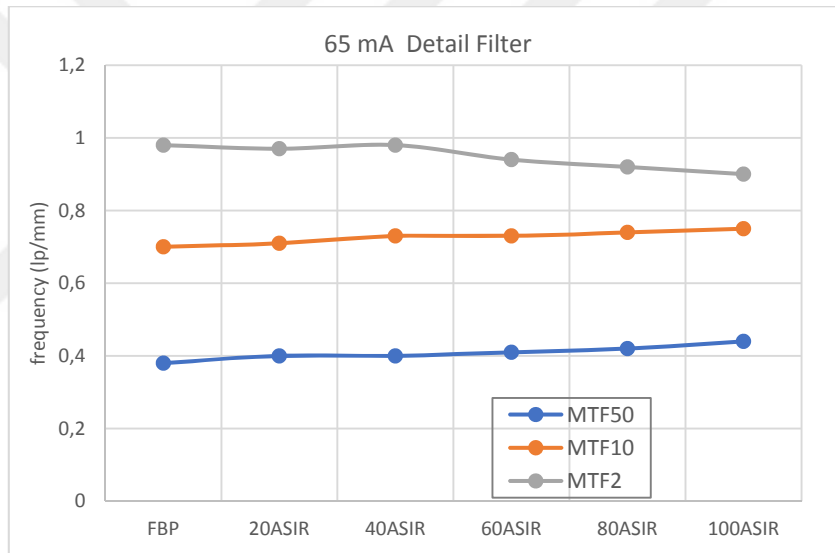


Figure A.4. MTF percentage graphs for detail filter



Figure A.5. MTF percentage values graphs for different slice thickness and reconstruction filters

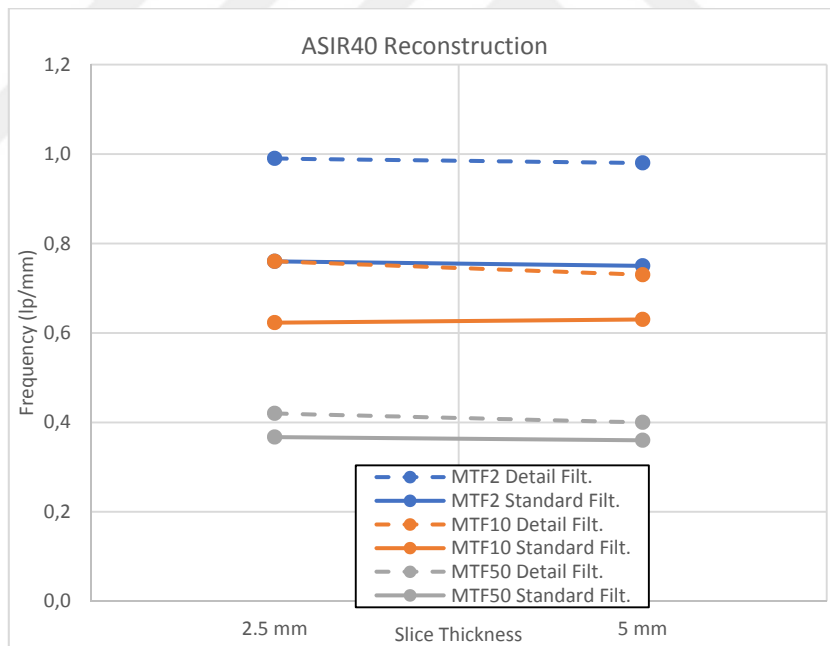


Figure A.6. MTF percentage values graphs for different slice thickness and ASIR40 filters

MTF Results for 65mA and 2.5 mm Slice Thickness

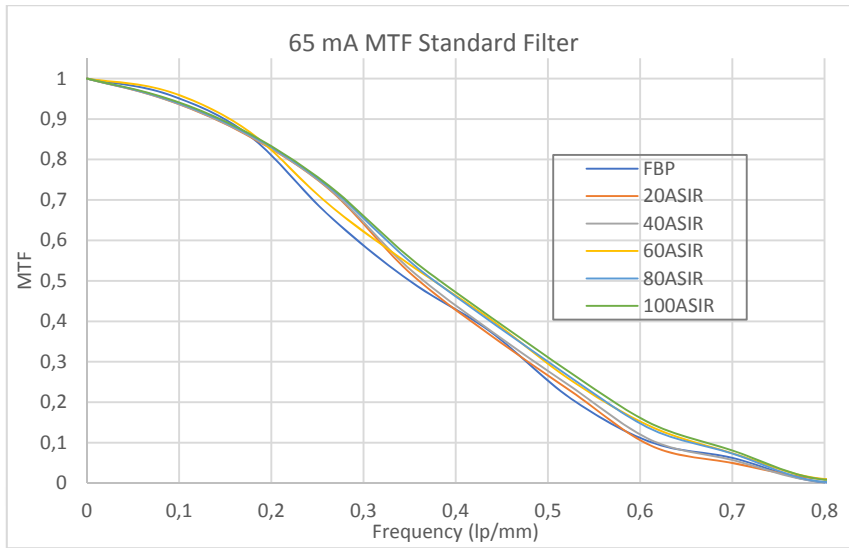


Figure A.7. MTF graphs for standard filter

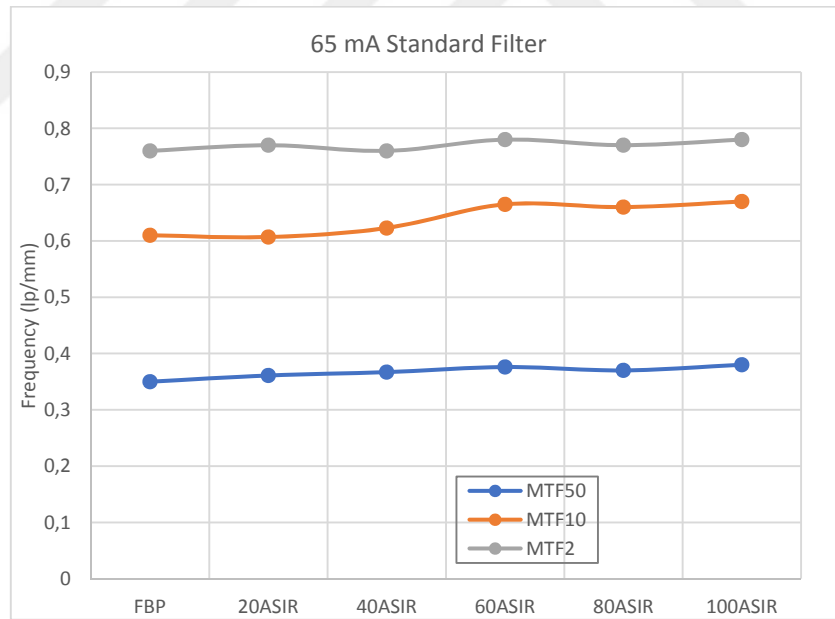


Figure A.8. MTF percentage graphs for standard filter

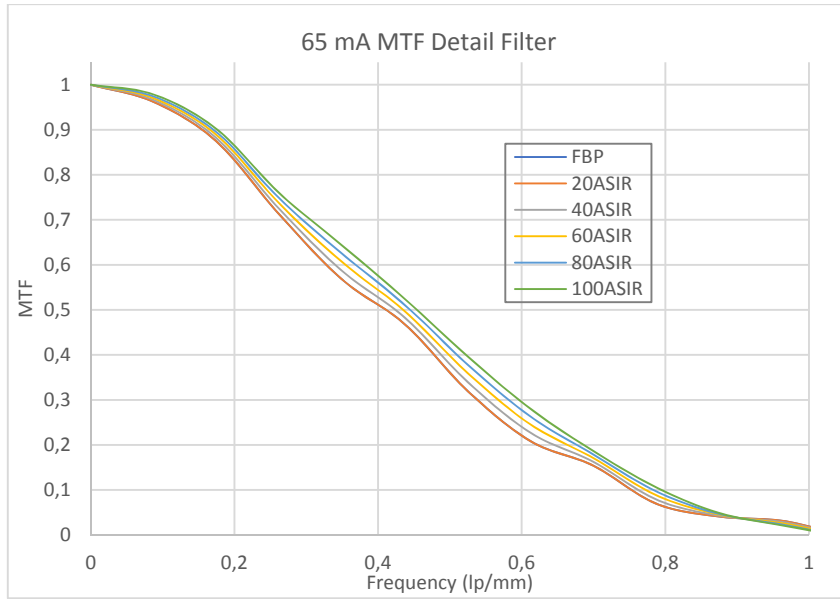


Figure A.9. MTF graphs for detail filter

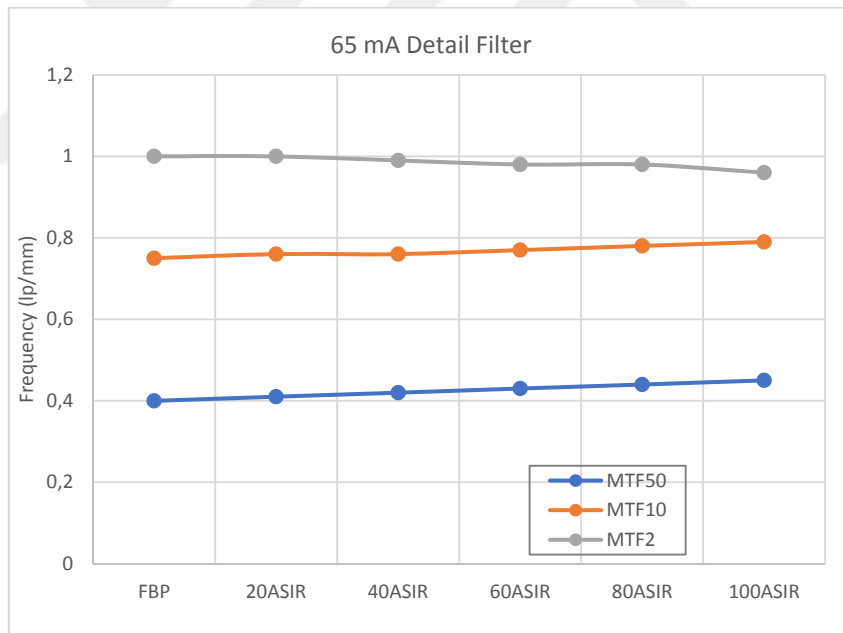


Figure A.10. MTF percentage graphs for detail filter

MTF Results for 255mA and 5 mm Slice Thickness

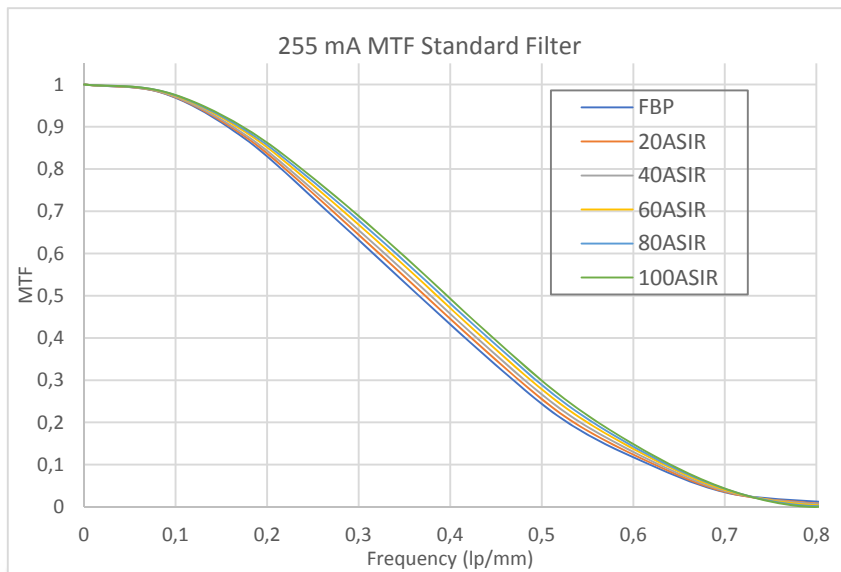


Figure A.11. MTF graphs for standard filter

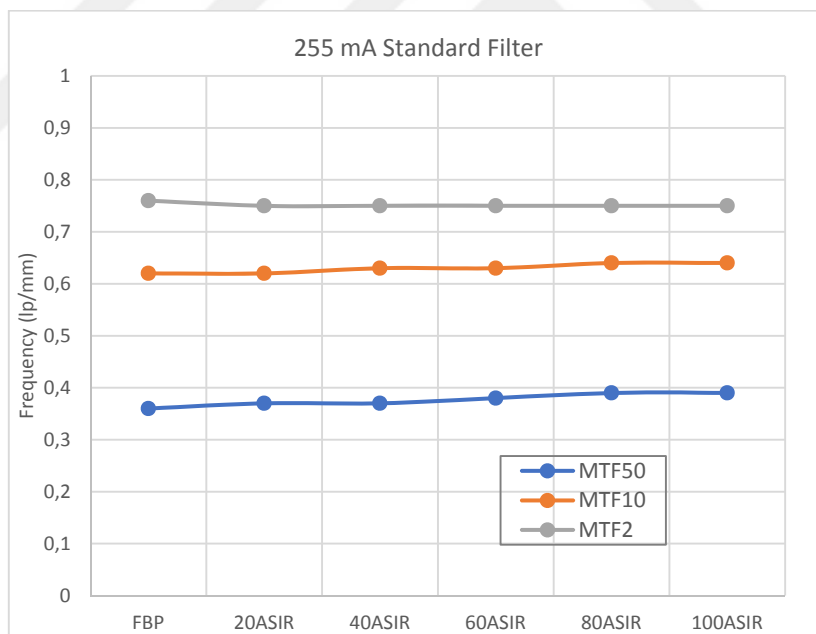


Figure A.12. MTF percentage graphs for standard filter

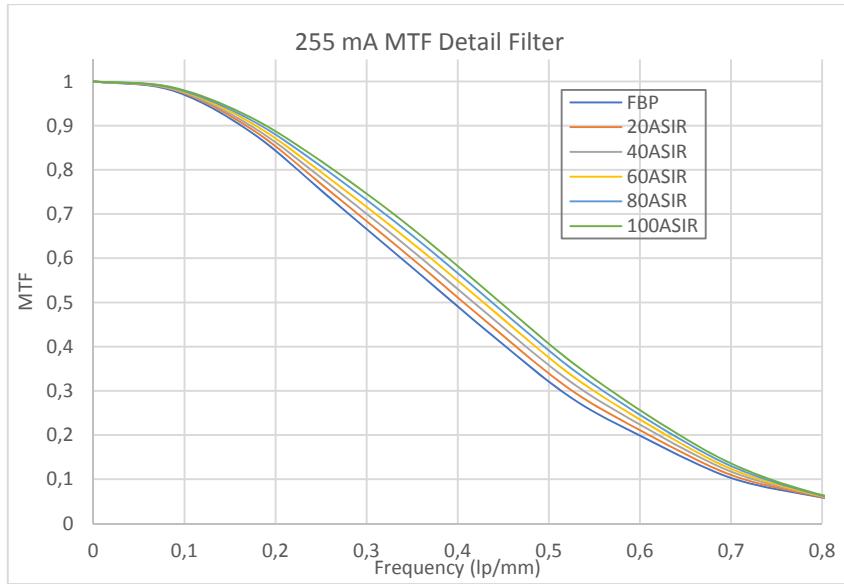


Figure A.13. MTF graphs for detail filter

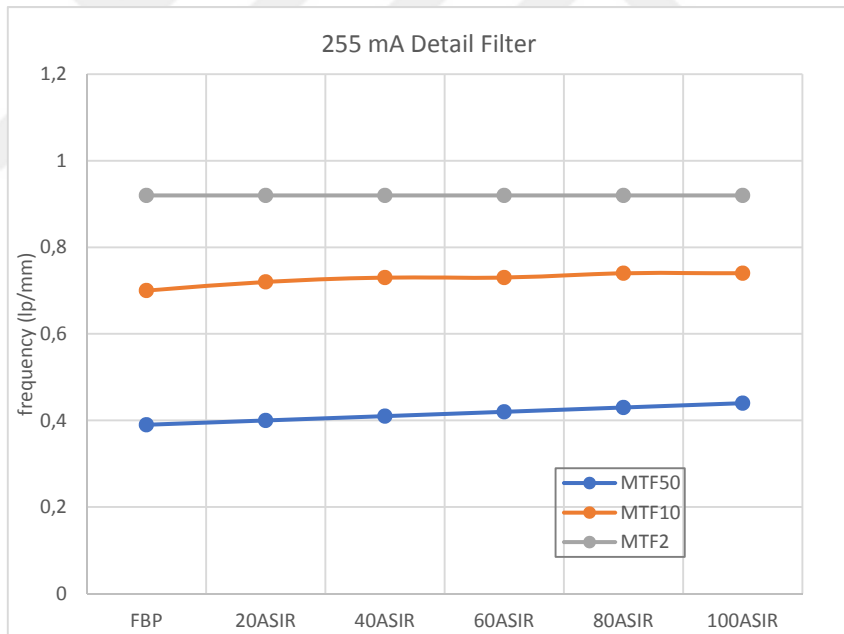


Figure A.14. MTF percentage graphs for detail filter

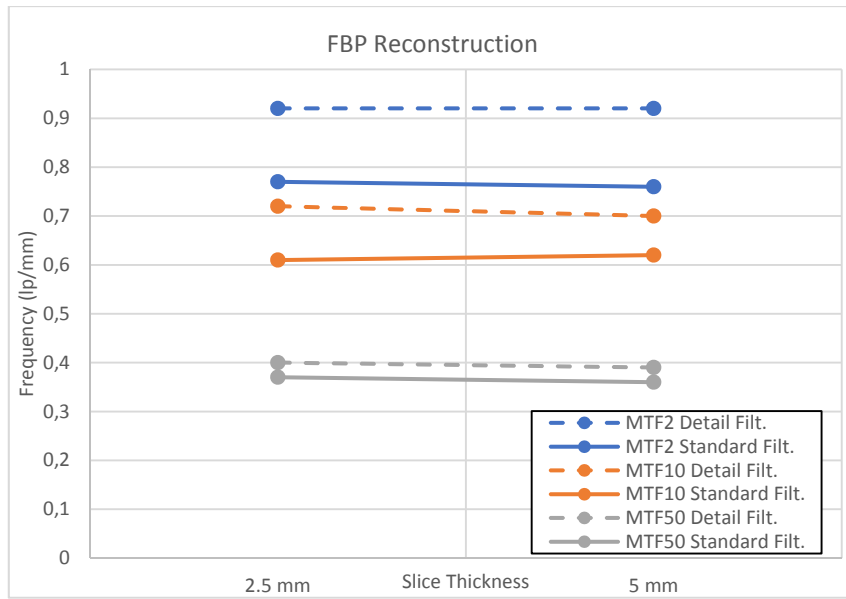


Figure A.15. MTF percentage values graphs for different slice thickness and reconstruction filters

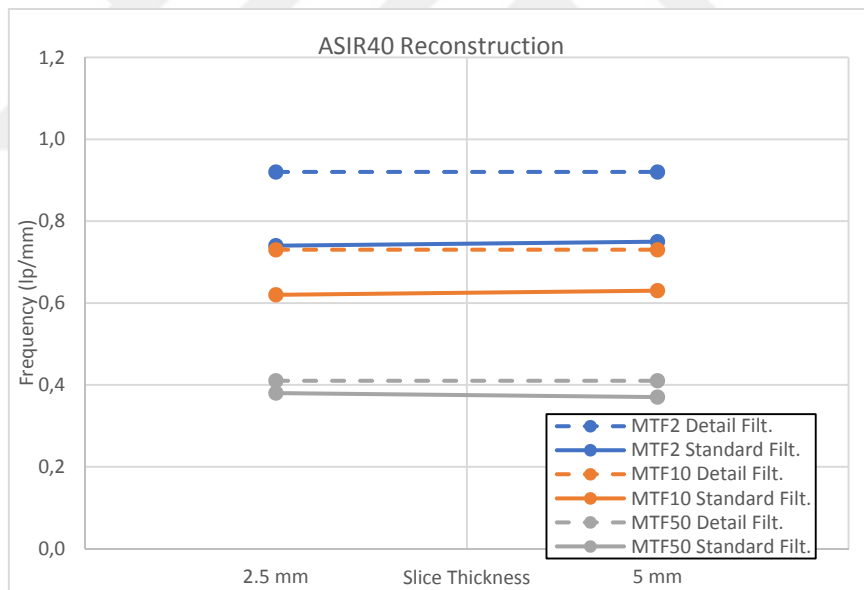


Figure A.16. MTF percentage values graphs for different slice thickness and ASIR40 filters

MTF Results for 255mA and 2.5 mm Slice Thickness

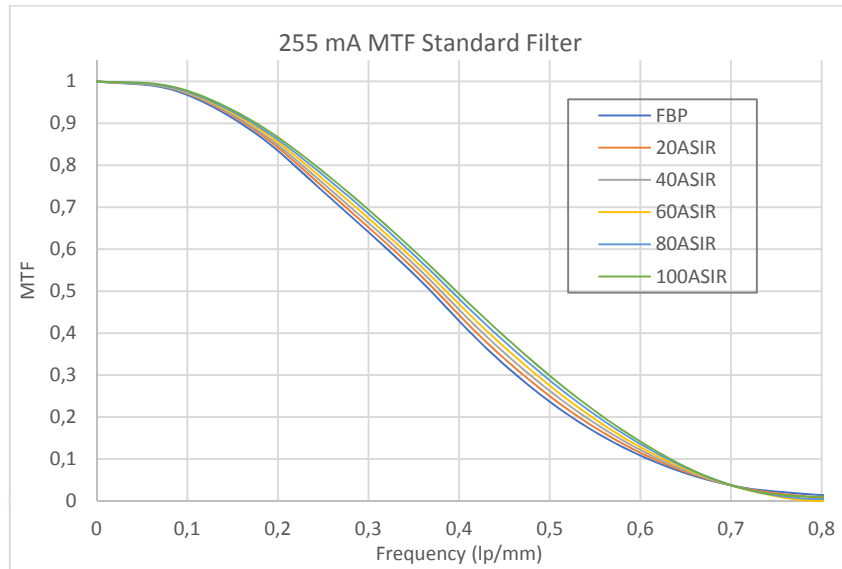


Figure A.17. MTF graphs for standard filter

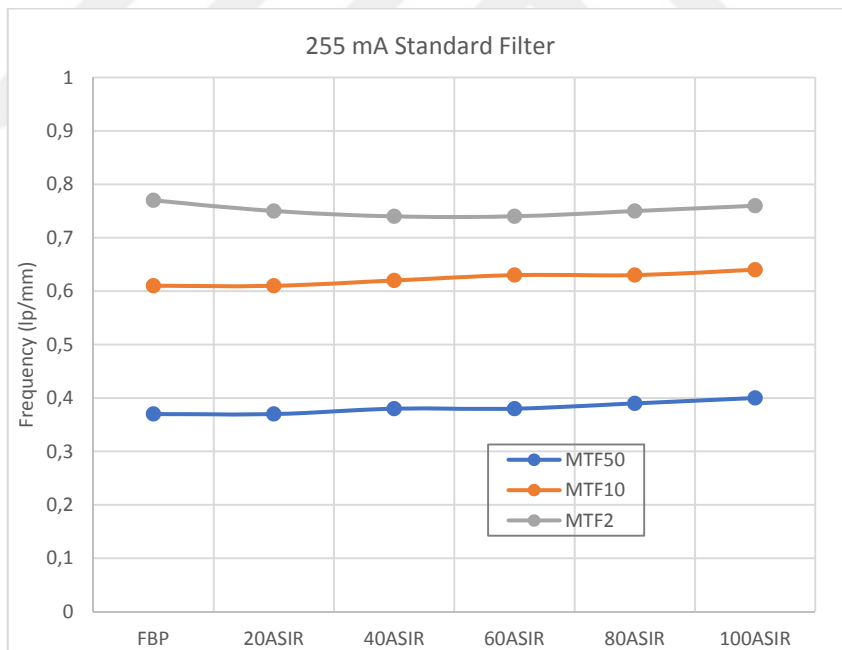


Figure A.18. MTF percentage graphs for standard filter

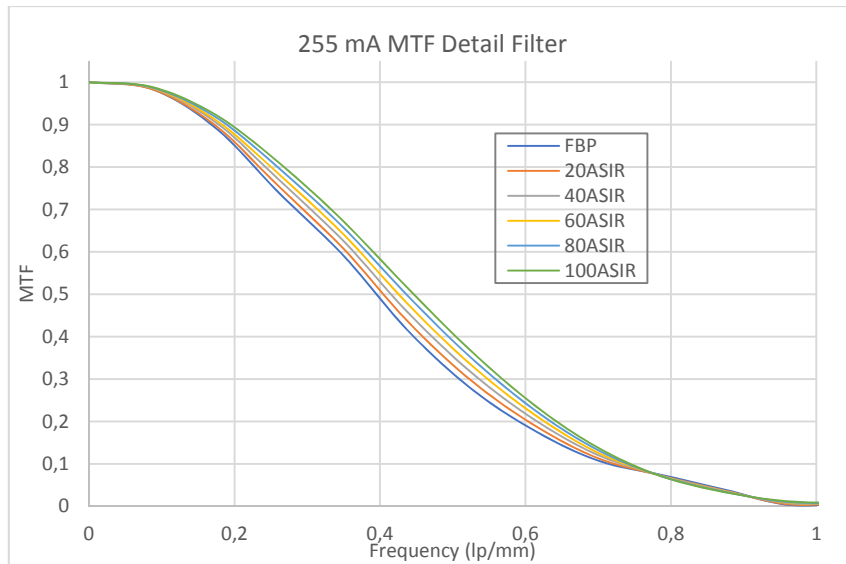


Figure A.19. MTF graphs for detail filter

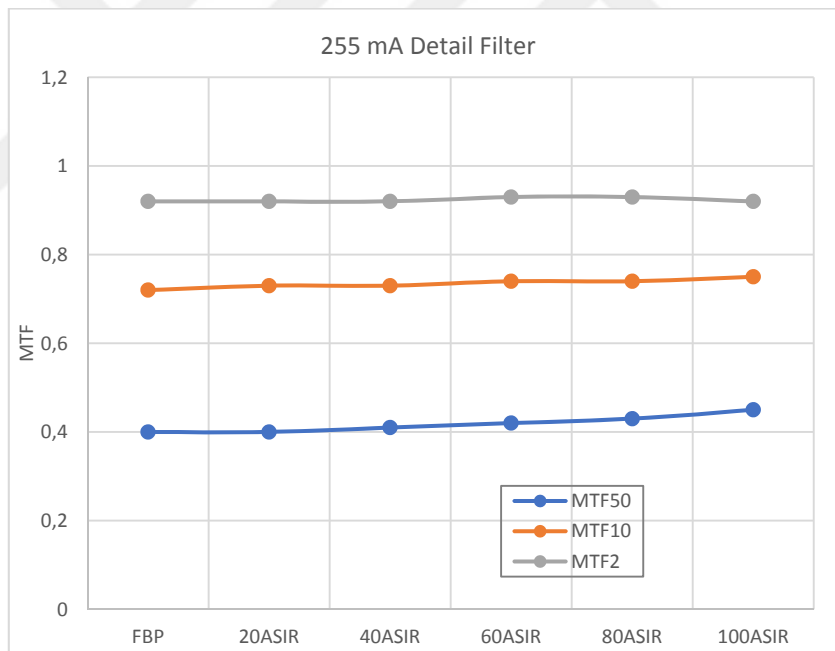
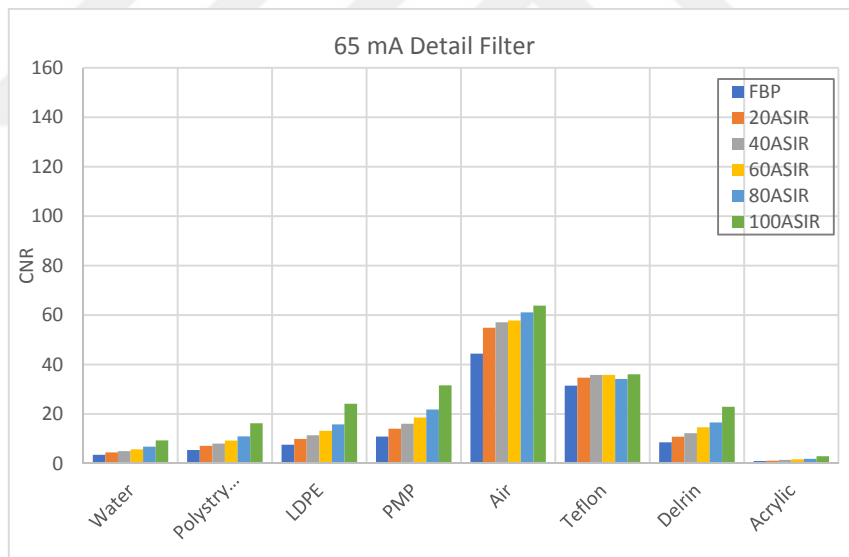
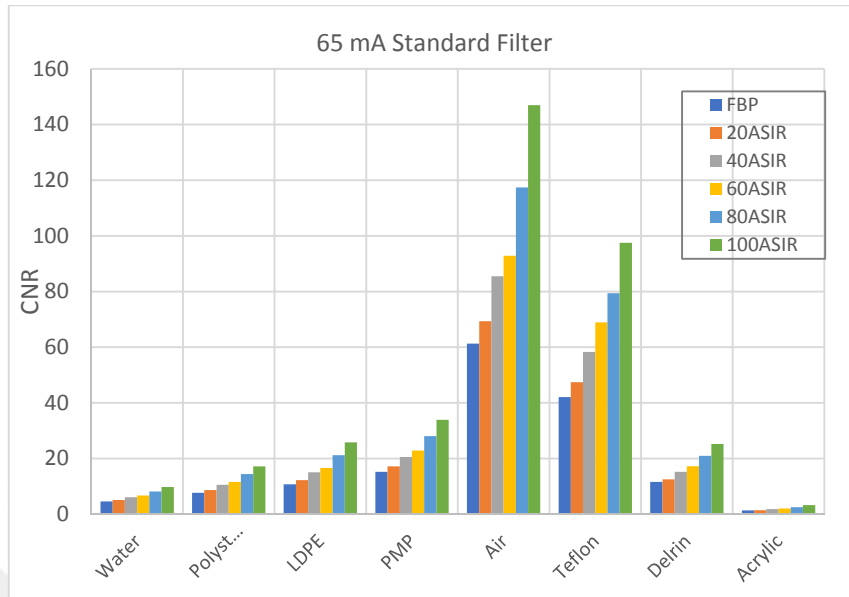
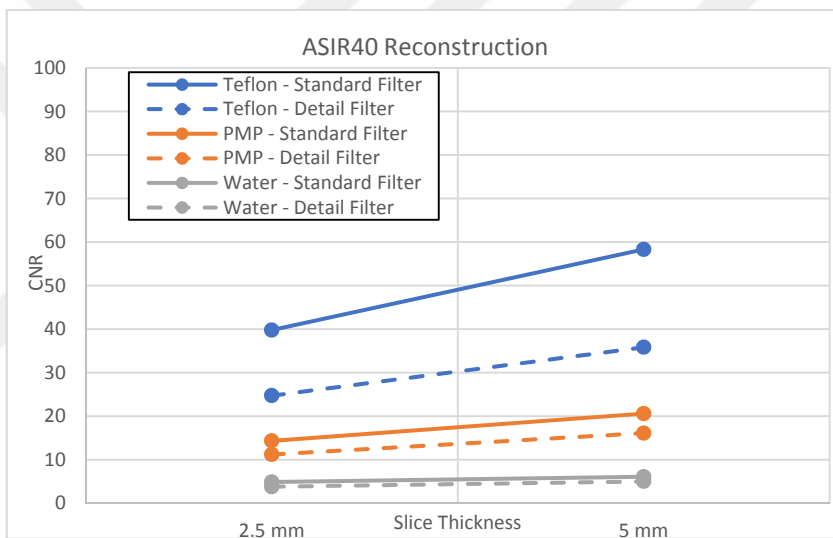
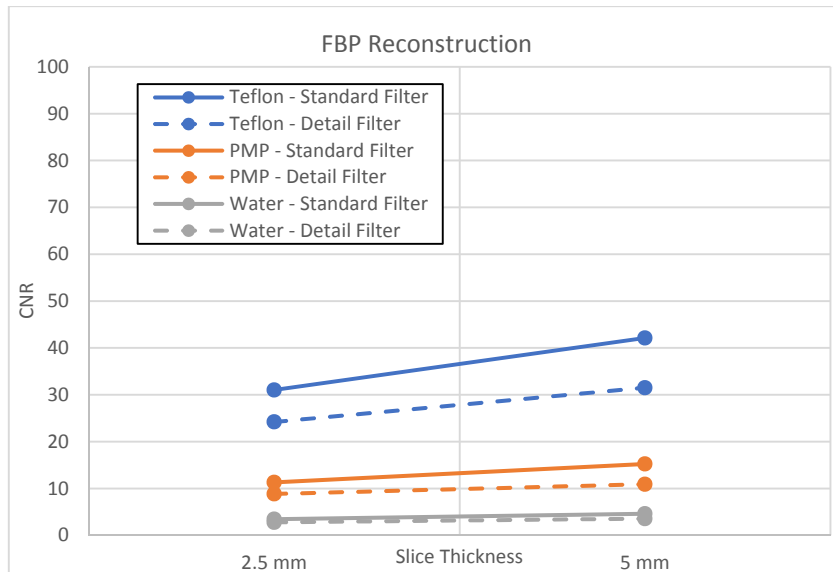


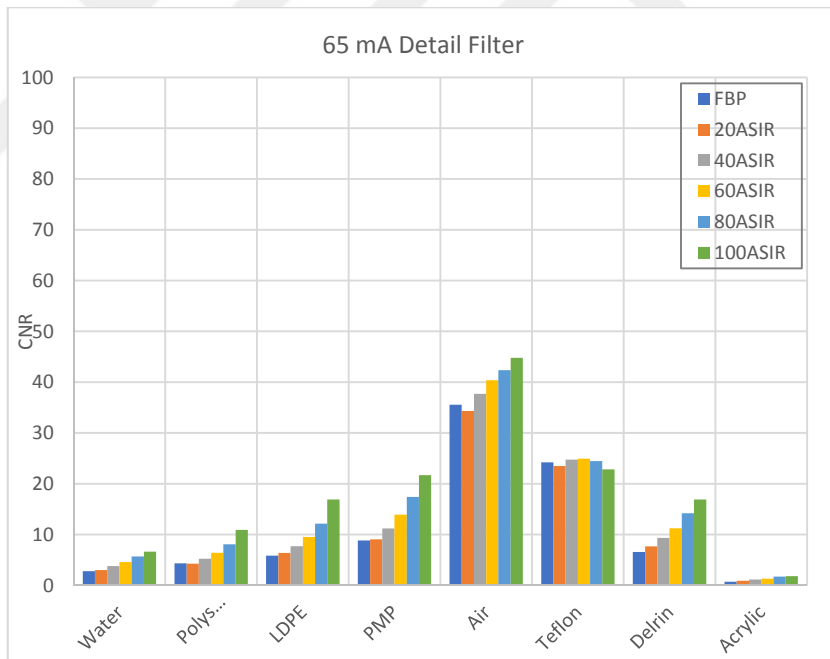
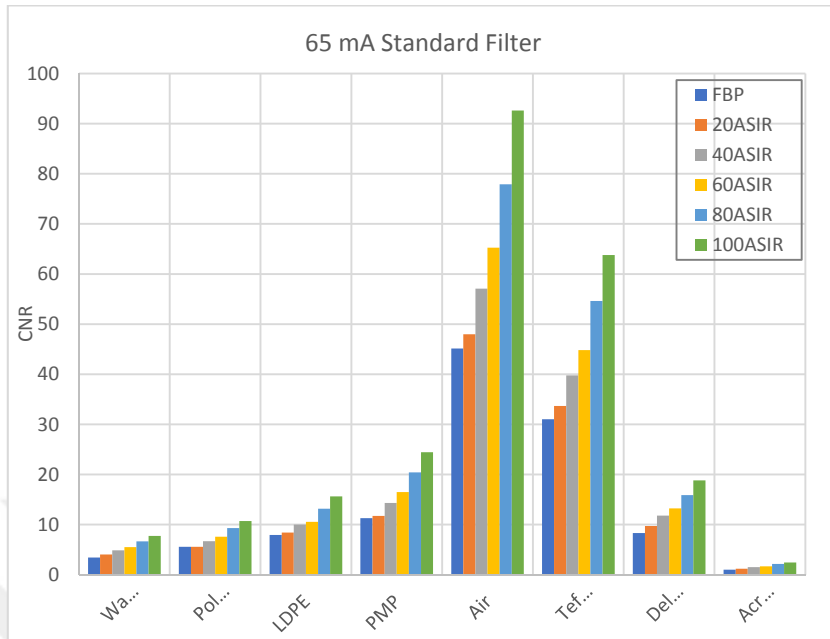
Figure A.20. MTF percentage graphs for detail filter

CNR Results for 65mA and 5 mm Slice Thickness

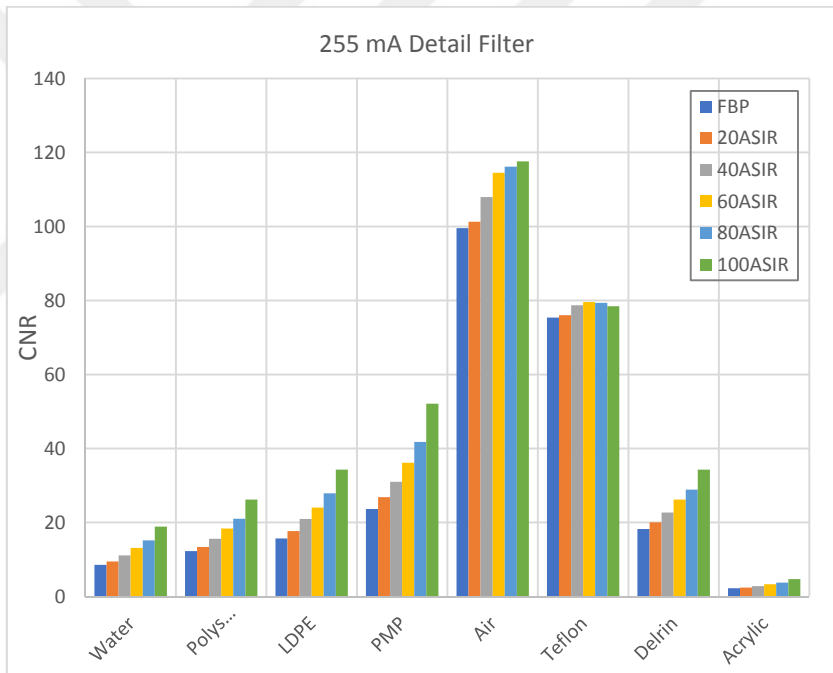
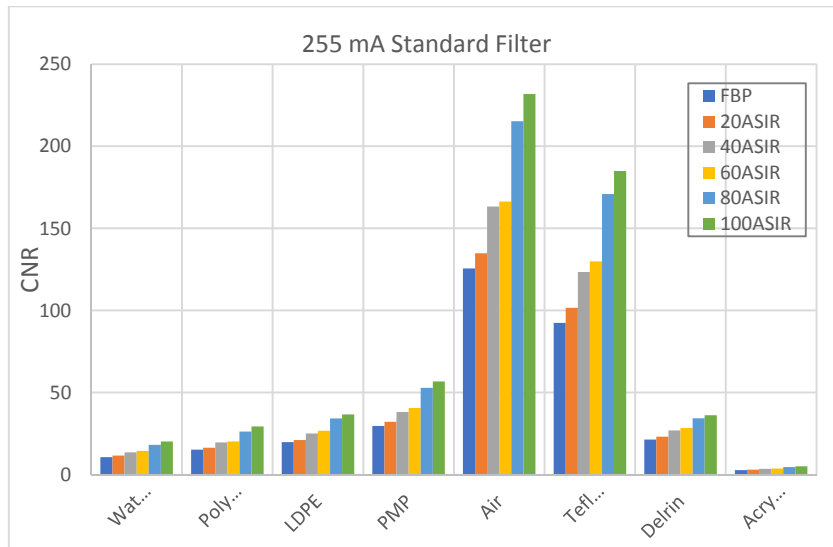


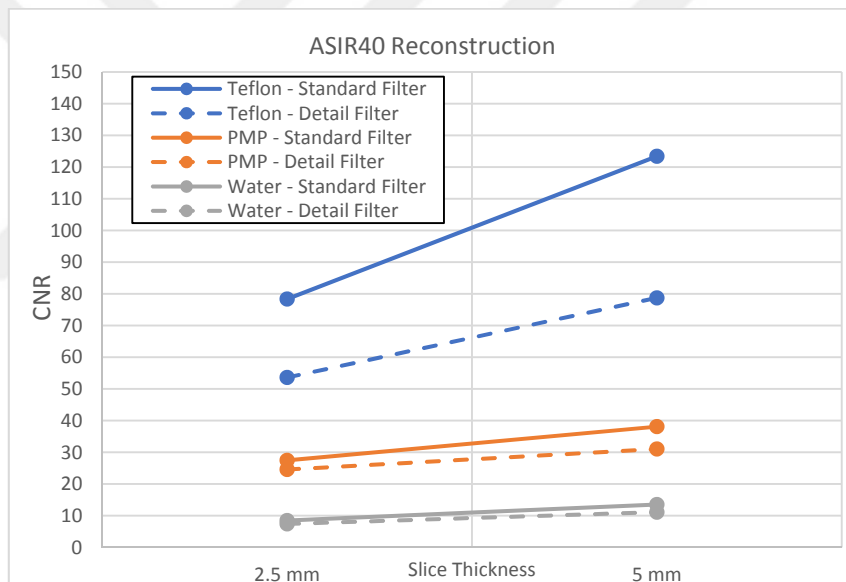
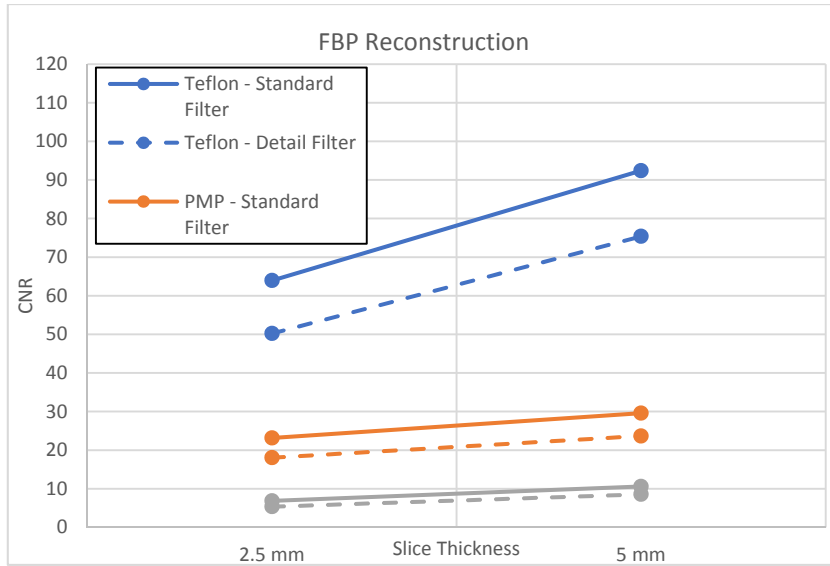


CNR Results for 65mA and 2.5 mm Slice Thickness

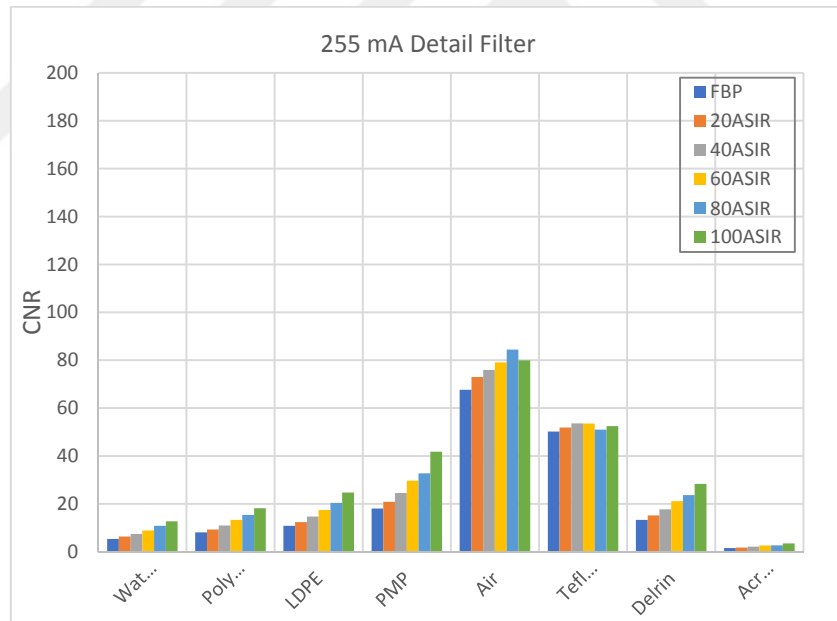
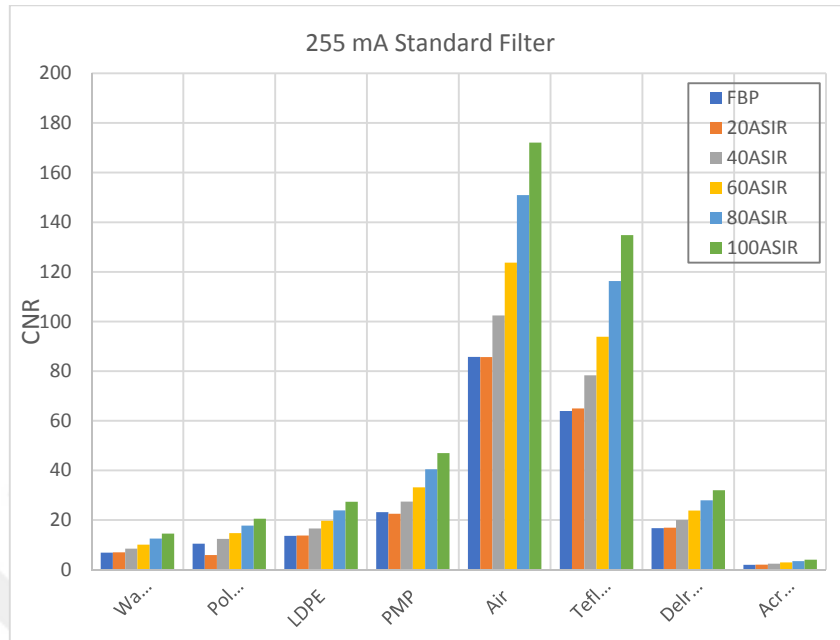


CNR Results for 255mA and 5 mm Slice Thickness

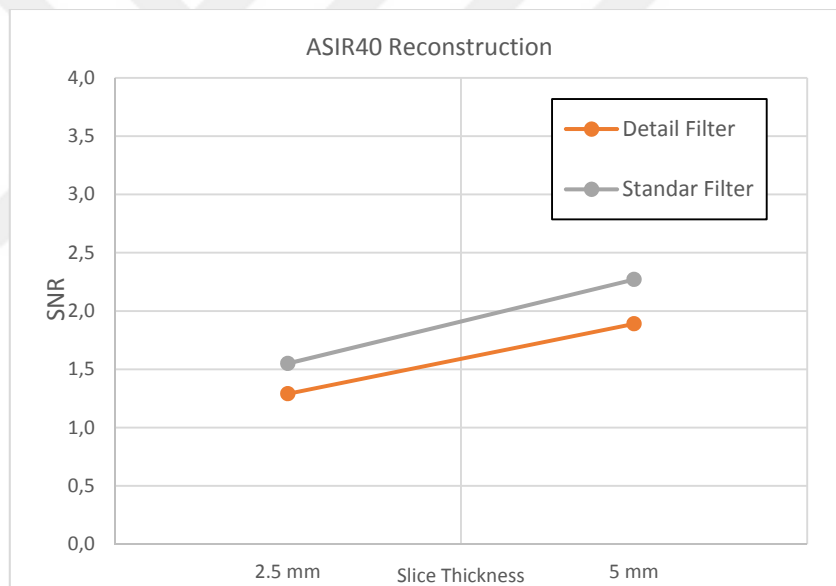
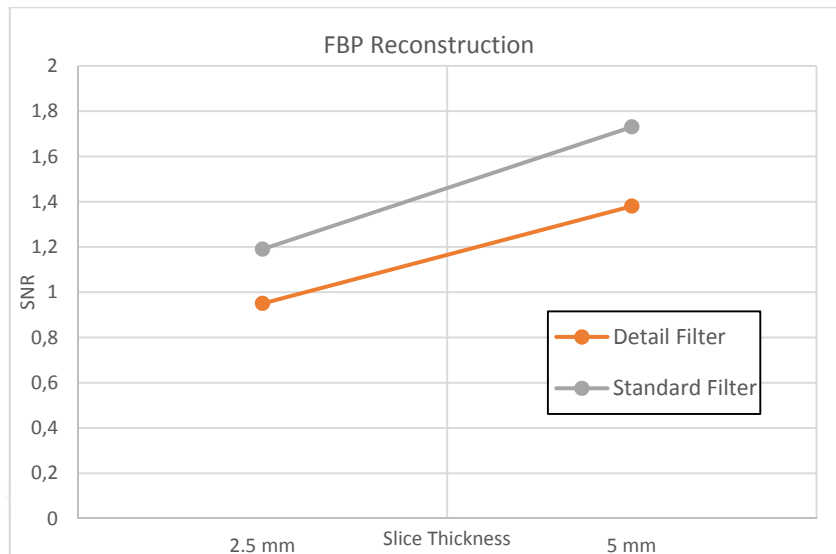




CNR Results for 255mA and 2.5 mm Slice Thickness



SNR Results for 65mA



SNR Results for 255mA

